THE STUDY OF PORPHYRINS CONFINEMENT IN NAFION MEMBRANE ***AND*** PHOTOVOLTAIC PROPERTIES OF A BULK HETEROJUNCTION SOLAR CELL

ADDIS ABABA UNIVERSITY
SCHOOL OF GRADUATE STUDIES

By: Girma Hailu

March, 2007

The Study of Porphyrins Confinement In Nafion membrane
And
Photovoltaic Properties of a Bulk Heterojunction Solar Cell

This thesis includes two independent parts which are carried out in two different Laboratories

Part - 1
The Study of Porphyrins Confinement in Nafion membrane

iThemba LABS, Cape Town, South Africa

Part - 2
Photovoltaic Properties of a Bulk Heterojunction Solar Cell

Conducting polymer laboratory, Addis Ababa University, Addis Ababa, Ethiopia

Part – 1

The Study of Porphyrins Confinement in Nafion membrane

iThemba LABS, Cape Town, South Africa

Part – 2

Photovoltaic Properties of a Bulk Heterojunction Solar Cell

Conducting polymer laboratory, Addis Ababa University, Addis Ababa, Ethiopia

THE STUDY OF PORPHYRINS CONFINEMENT IN NAFION MEMBRANE AND PHOTOVOLTAIC PROPERTIES OF A BULK HETEROJUNCTION SOLAR CELL

By
Girma Hailu

A THESIS PRESENTED TO
THE SCHOOL OF GRADUATE STUDIES
ADDIS ABABA UNIVERSITY
IN PARTIAL FULFILLMENT OF THE REQUIREMENTS
FOR THE DEGREE OF

MASTER OF SCIENCE in PHYSICS

ADDIS ABABA, ETHIOPIA
APRIL 2007

ADDIS ABABA UNIVERSITY

DEAPRMENT OF PHYSICS

The undersigned hereby certify that they have read and recommend to the Faculty of Science for acceptance a senior project entitled "**The study of Porphyrins confinement in Nafion membrane and Photovoltaic Properties of a Bulk Heterojunction Solar Cell**" by **Girma Hailu Master of Science**.

Dated: April 2007

Supervisor: _____
Dr. Genene Tessema / Dr. Malik Maaza

Examiners: _____
Dr. Gizaw Mengistu

_____
Dr. S. K. Ghoshal

This Work is Dedicated to
My Dear Mother: Askale Bereka

Table of Contents

List of Tables

List of Figures

Acknowledgements

I am very grateful to NANO-AFNET for the financial support that I received in order to conduct this research in iThemba LABS, Cape Town, South Africa. I want to thank Dr. Genene Tessema for his unlimited support, wise advise and strong motivation through out the process of this study. I also want to thank Dr. Malik Maaza for hosting and advising me in the material research group at iThemba LABS. I want to appreciate his brilliant ideas which I was following while doing the research. Many thanks goes to the university of Western Cape (UWC) and Stallenbousch University for their cooperation to use their facilities. The constructive discussions that I have had with my friends Balla Diop Ngom and Tesfaye Mamuye put significant inputs for the successful completion of this study. At last, but certainly not the least I want to thank my **God** for giving me the strength and courage to complete this task.

Addis Ababa University

March, 2007

Abstract

With the development of strong laser sources for different applications which in some instances has extremely high intensity, optical power limiters are needed to provide human eye and optical detector protection. So, a smart ultra fast optical power limiter that is transparent for low incident intensities and blocks the output at high input intensities is required. The operation of optical power limiters is based on the phenomena of nonlinear absorption (NLA). Different Porphyrins have been reported to have NLA property which put them as potential candidate for application as optical power limiters. In this paper, we have investigated NLA and optical limiting properties of five different types of Porphyrins by using the Z-scanning technique. The Porphyrins were confined into Nafion membrane in order to protect them from possible degradation. The results of the experiments clearly show the fascinating NLA and optical power limiting properties of the Porphyrins under investigation. By fitting the Z-scan results with the theoretical fitting function, the nonlinear absorption coefficients (β) of all the Porphyrins with different concentrations for each of them is determined. Besides, their linear absorption coefficients are obtained by considering low intensity regimes from the data and applying Beer's low of linear absorption.

Chapter 1

Introduction

Porphyrins and their derivatives posses great application potential for a variety of purposes. The nonlinear optical properties of these materials are of especial interest, partly due to their ability to transfer energy with in molecular control, and partly for their potential in applications such as optical communications, data storage, and electro optical signal processing. This is due to the fact that they have great thermal stability and extended π-conjugated macro cyclic ring which give them large nonlinear optical (NLO) effects. This strong NLO property makes them even more important for optical switching and optical limiting materials.

When considering a material as an optical limiter, two properties that are of particular interest are the material's nonlinear absorption coefficient and its nonlinear index of refraction. Both change the intensity of the light in a nonlinear way as it passes through the medium. By measuring the nonlinear properties of the materials, they can be identified as possible optical limiters.

The development of more powerful lasers for applications such as laser ablation and the air-borne laser make optical limiters essential to provide human eye and optical detector protection. The light intensity may be randomly fluctuating so that it could be extremely high at times and low at other times. In order to rectify such high intensity fluctuation of the laser one can use a notch filter to remove a narrow band of wave lengths. However, wavelength agile lasers now available are making

this strategy useless. However, a smart optical limiter which is transparent for low input intensities and blocks the output at high input intensities is needed that could also be effective over a wide band of wave lengths. The ideal solution would be a passive optical limiter with a fast response since mechanical or electrical switches and controller circuits could not respond fast enough for ultra fast pulse inputs. The operation of optical power limiters is usually based on the phenomena of NLA. They use sequential multiphoton absorption [1,2,3], simultaneous multiphoton absorption, thermal lensing effect and optically induced molecular reorientation in liquid crystal, etc.

Chapter 2

Theory of nonlinear optical processes in matter

In the discussion of nonlinear optical processes in materials, it is necessary to have a general theoretical understanding of these processes. In this chapter a very concise framework of this theory based on Maxwell's equations is presented [4].

2.1 Theoretical framework for nonlinear light-matter interactions

It is customary to start with Maxwell's equations when describing any light-matter interaction.

$$\nabla \times \mathbf{H} = \frac{\partial \mathbf{D}}{\partial t} \tag{2.1}$$

$$\nabla \cdot \mathbf{D} = 0 \tag{2.2}$$

$$\nabla \times \mathbf{E} = -\frac{\partial \mathbf{B}}{\partial t} \tag{2.3}$$

$$\nabla \cdot \mathbf{H} = 0 \tag{2.4}$$

In these equations, it has been assumed that the surface charge density(σ) and the volume charge density (ρ) are both zero. It is important to note that the magnetic field, $\mathbf{B}$, and $\mathbf{H}$ are related through $\mathbf{B} = \mu_o \mathbf{H}$, where μ_o being the permeability of free space,

and that the electric field (**E**) and the electric displacement (**D**) are related through $\mathbf{D}(\mathbf{E}) = \epsilon_o\mathbf{E}+\mathbf{P}(\mathbf{E})$. Where the dielectric polarization $\mathbf{P}(\mathbf{E})$ is the dipole moment per unit volume, and ϵ_o is the permittivity of free space. Light-matter interactions are usually considered within the framework of the Lorentz model [5]. In the Lorentz model, the electrons are considered to be bound to the atom in a harmonic potential. This is equivalent to expressing the polarization of the material as a result of an electric field as

$$\mathbf{P}(\mathbf{E}) \;=\; \epsilon_o\chi^{(1)}\mathbf{E} \tag{2.5}$$

where $\chi^{(1)}$ is the linear susceptibility of the material. This accounts accurately for all linear phenomena occurring during light-matter interactions. This, however, does not explain the nonlinear phenomena observed when high intensity light interacts with matter. To explain this, it is necessary to consider the electron to be bound in a more generalized potential, namely as unharmonic potential. This potential can be approximated by series of expansion at low energies to a harmonic potential. For this discussion the approach of Milonni and Eberly [5] is followed. This general potential is normally expressed as a power series

$$V(x) \;=\; \frac{1}{2}m\omega_o^2x^2 + Ax^3 + Bx^4 + \cdots \tag{2.6}$$

in which the first term is the harmonic potential, which dominates the expression for small displacements, x. This can be obtained in the following way. Whatever the true potential is, it can be expanded in a Taylor series in the normal fashion

$$V(x) \;=\; V(0) + x\left(\frac{dV}{dx}\right)_{x=0} + \frac{1}{2!}x^2\left(\frac{d^2V}{dx^2}\right)_{x=0} + \frac{1}{3!}x^3\left(\frac{d^3V}{dx^3}\right)_{x=0} + \cdots \tag{2.7}$$

about the equilibrium point, $x = 0$. $V(0)$ is just an additive constant to the total energy and does not give rise to any force ($F = -dV/dx$). The constant term can therefore be neglected.

$$\left(\frac{dV}{dx}\right)_{x=0} \;=\; 0 \tag{2.8}$$

and that

$$\left(\frac{d^2V}{dx^2}\right)_{x=0} \;>\; 0 \tag{2.9}$$

The result is that equation 2.7 can be rewritten as

$$V(x) \;=\; \frac{1}{2}x^2\left(\frac{d^2V}{dx^2}\right)_{x=0} + \frac{1}{6}x^3\left(\frac{d^3V}{dx^3}\right)_{x=0} + \cdots \tag{2.10}$$

and since $d^2V/dx^2 > 0$, we can define

$$m\omega_o^2 \;\equiv\; \left(\frac{d^2V}{dx^2}\right)_{x=0} \tag{2.11}$$

In a similar fashion, we define

$$A \;=\; \frac{1}{6}\left(\frac{d^3V}{dx^3}\right)_{x=0} \tag{2.12}$$

This can be done for all the terms in Equation 2.6. Therefore, the force on an electron in this potential is given by

$$\mathbf{F} \;=\; -\frac{dV}{dx} \;=\; -m\omega_o^2 x - 3Ax^2 - 4Bx^3 - \cdots \tag{2.13}$$

which implies

$$\ddot{x} + \omega_o^2 x + \frac{3A}{m}x^2 + \frac{4B}{m}x^3 + \cdots \;=\; \frac{e}{m}\mathbf{E}(t) \tag{2.14}$$

when considering Newtons equations of motion. This is a nonlinear differential equation, which is generally not possible to solve analytically. The polarization density (**P**) is given by

$$\mathbf{P} \;=\; Ne\hat{x} \tag{2.15}$$

where N is the number of molecules per unit volume. Considering potential solutions for Equation 2.14 and substituting them into Equation 2.15 leads to a power series in **E** for the polarization, **P** [6].

$$\mathbf{P}(\mathbf{E}) \;=\; \epsilon(\chi^{(1)}\mathbf{E} + \chi^{(2)}\mathbf{E}^2 + \chi^{(3)}\mathbf{E}^3 + \cdots) \tag{2.16}$$

The expansion coefficients ($\chi^{(n)}$) are tensors (Equation 2.16) therefore represents a tensor product and are the dielectric susceptibilities which are intrinsic properties of the material. As was mentioned, $\chi^{(1)}$ is the linear susceptibility. It is a complex number that governs the linear optical processes in the material, the real part being

related to the linear index of refraction, n, and the imaginary part related to the linear absorption coefficient, α. All the other $\chi^{(n)}$ are the higher order susceptibilities that govern the nonlinear processes. They are not significant in the linear regime because of their relative strengths. If it is considered that $\chi^{(1)} = 1$, then the relative strengths of the higher order susceptibilities are typically of the order, $\chi^{(2)} \approx 10^{-10} cm/V$ and $\chi^{(3)} \approx 10^{-17} cm^2/V^2$. It is thus clear that only when the intensity of the incident light is sufficiently high, then the higher order polarization terms become significant. In general, all the susceptibilities are tensors. They take into account of the polarization of the incident electric fields relative to the orientation of the medium. Generally, if the medium is anisotropic and hence responds differently for different polarization directions of the incident fields. However, it is not necessary to consider them as tensors for this discussion, since their tensor character is not essential for this analysis.

The different orders of susceptibilities govern different processes that occur during the interaction of light with matter. The number of waves or photons that participate in an interaction determine which $\chi^{(n)}$ describes the interaction. For instance, $\chi^{(1)}$ describes two-wave interactions, $\chi^{(2)}$ three-wave, $\chi^{(3)}$ four-wave and so forth. A three-wave interaction implies that two waves (with frequencies ω_1 and ω_2) enter the medium and one (with frequency ω_3) leaves, or one wave enters the medium and two leave the medium.

Energy, momentum and angular momentum must be conserved during these interactions. For the above example energy conservation implies that $\omega_3 = \omega_1 + \omega_2$ or $\omega_3 = \omega_1 - \omega_2$. In a degenerate case, where $\omega_1 = \omega_2$, as this is the case when only a single frequency laser is incident on the material. This implies that $\omega_3 = 2\omega_1$, and this is known as second harmonic generation. For a four-wave interaction, three waves are incident on the sample and one exits the sample. In this case $\chi^{(3)}$ describes the interaction. If all the incident waves have the same frequency, then the wave that exit the material can have a frequency three times the incident frequency (third harmonic generation) or equal to the incident frequency ($\omega_4 = \omega_1 - \omega_1 + \omega_1 = \omega_1$). In cases where the exiting wave and the incident wave are of the same frequency and nonlinear interactions has occurred, then, the process therefore be described by at least the $\chi^{(3)}$

term, but cannot be described by a lower order term. An example of this is self focussing, which will be discussed in detail in section 2.2.

To describe nonlinear light-matter interactions it is necessary to find a solution for Maxwell's equations (Equations 2.1 to 2.4), where the nonlinear polarization is now included. It is customary to separate the linear part from the nonlinear part by rewriting the polarization (Equation 2.16) in the form

$$\mathbf{P}(\mathbf{E}) \;=\; \epsilon_o(\epsilon_1 - 1)\mathbf{E} + \mathbf{P}_{NL} \tag{2.17}$$

with ϵ_1 the linear dielectric constant,

$$(\epsilon_1 - 1) \;=\; \chi^{(1)}$$

$$\epsilon_1 \;=\; \chi^{(1)} + 1 \tag{2.18}$$

and $\mathbf{P}_{NL}$ containing all the higher order polarization terms. In this form the electric displacement simply becomes

$$\mathbf{D}(\mathbf{E}) \;=\; \epsilon_o\epsilon_1\mathbf{E} + \mathbf{P}_{NL} \tag{2.19}$$

Maxwell's equations, including the nonlinear polarization term, can now be written as

$$\nabla \times \mathbf{H} \;=\; \frac{\partial}{\partial t}(\epsilon_o\epsilon_1\mathbf{E} + \mathbf{P}_{NL}) \;=\; \epsilon_o\epsilon_1\frac{\partial \mathbf{E}}{\partial t} + \frac{\partial \mathbf{P}_{NL}}{\partial t} \tag{2.20}$$

$$\nabla \times \mathbf{E} \;=\; -\frac{\partial}{\partial t}(\mu_o\mathbf{H}) \;=\; -\mu_o\frac{\partial \mathbf{H}}{\partial t} \tag{2.21}$$

The last set of coupled differential equations must be solved inorder to extract the nonlinear wave equation. We start by simplifying the curl of Equation 2.21.

$$\nabla \times \nabla \times \mathbf{E} \;=\; \nabla \times \left(-\mu_o\frac{\partial \mathbf{H}}{\partial t}\right) \;=\; -\mu_o\frac{\partial}{\partial t}(\nabla \times \mathbf{H}) \tag{2.22}$$

Substituting Equation 2.20 into Equation 2.22 yields

$$\nabla \times \nabla \times \mathbf{E} \;=\; -\mu_o \frac{\partial}{\partial t}\left(\epsilon_o \epsilon_1 \frac{\partial \mathbf{E}}{\partial t} + \frac{\partial \mathbf{P}_{NL}}{\partial t}\right) \tag{2.23}$$

Using the general identity $\nabla \times (\nabla \times \mathbf{E}) \;=\; \nabla(\nabla \cdot \mathbf{E}) - \nabla^2 \mathbf{E}$ Equation 2.23 is rewritten as

$$\nabla(\nabla \cdot \mathbf{E}) - \nabla^2 \mathbf{E} \;=\; -\mu_o \frac{\partial}{\partial t}\left(\epsilon_o \epsilon_1 \frac{\partial \mathbf{E}}{\partial t} + \frac{\partial \mathbf{P}_{NL}}{\partial t}\right) \tag{2.24}$$

In general only transverse fields are considered, which implies that $\nabla \cdot \mathbf{E} = 0$. This simplifies Equation 2.24 as follows,

$$\nabla^2 \mathbf{E} \;=\; \mu_o \frac{\partial}{\partial t}\left(\epsilon_o \epsilon_1 \frac{\partial \mathbf{E}}{\partial t} + \frac{\partial \mathbf{P}_{NL}}{\partial t}\right)$$

$$\nabla^2 \mathbf{E} \;=\; \epsilon_o \mu_o \epsilon_1 \frac{\partial^2 \mathbf{E}}{\partial t^2} + \mu_o \frac{\partial^2 \mathbf{P}_{NL}}{\partial t^2}$$

$$\nabla^2 \mathbf{E} \;=\; \frac{\epsilon_1}{c^2}\frac{\partial^2 \mathbf{E}}{\partial t^2} + \frac{1}{c^2 \epsilon_o}\frac{\partial^2 \mathbf{P}_{NL}}{\partial t^2}$$

$$\nabla^2 \mathbf{E} - \frac{\epsilon_1}{c^2}\frac{\partial^2 \mathbf{E}}{\partial t^2} \;=\; \frac{1}{c^2 \epsilon_o}\frac{\partial^2 \mathbf{P}_{NL}}{\partial t^2}, \tag{2.25}$$

where the fact that $\epsilon_o \mu_o = c^{-2}$, with c being the speed of light in vacuum, is used. Equation 2.25 is known as the nonlinear inhomogeneous wave equation [7]. To obtain a solution of the nonlinear wave equation, it is assumed that the solution consists of a linear summation of plane waves with discrete frequency components. The frequencies of these plane waves are ω_j and the accompanying wave vectors are $k_j = \frac{n_j \omega_j}{c}$. If it is further assumed that the plane waves only propagate along the z-axis, then the solutions can be described by [6]

$$\mathbf{E}(z,t) \;=\; \frac{1}{2}\left(\sum_{j=1}^{N} \mathbf{E}_j(z,t) e^{i(k_j z - \omega_j t)} + c.c.\right) \tag{2.26}$$

where c.c. refers to the complex conjugate of the first term and describes the waves

travelling in the negative direction. In a completely analogous fashion [6] the nonlinear polarization can be written as

$$\mathbf{P}(z,t) \;=\; \frac{1}{2}\left(\sum_{j=1}^{N}\mathbf{P}_j(z,t)e^{-i\omega_j t} + c.c.\right) \tag{2.27}$$

Since the complex conjugate terms only describe waves travelling in the negative direction, they do not yield any additional information. They are therefore discarded in the rest of the discussion. Taking the second order spatial derivative of the electric field and the second order temporal derivative of both the electric field and nonlinear polarization yields

$$\frac{\partial^2\mathbf{E}(z,t)}{\partial z^2} \;=\; \frac{1}{2}\sum_{j=1}^{N}\left(\frac{\partial^2\mathbf{E}_j}{\partial z^2} + 2ik_j\frac{\partial\mathbf{E}_j}{\partial z} - k_j^2\mathbf{E}_j\right)e^{ik_j z}e^{-i\omega_j t} \tag{2.28}$$

$$\frac{\partial^2\mathbf{E}(z,t)}{\partial t^2} \;=\; \frac{1}{2}\sum_{j=1}^{N}\left(\frac{\partial^2\mathbf{E}_j}{\partial t^2} - 2i\omega_j\frac{\partial\mathbf{E}_j}{\partial t} - \omega_j^2\mathbf{E}_j\right)e^{ik_j z}e^{-i\omega_j t} \tag{2.29}$$

$$\frac{\partial^2\mathbf{P}_{NL}(z,t)}{\partial t^2} \;=\; \frac{1}{2}\sum_{j=1}^{N}\left(\frac{\partial^2\mathbf{P}_{NL_j}}{\partial t^2} - 2i\omega_j\frac{\partial\mathbf{p}_{NL_j}}{\partial t} - \omega_j^2\mathbf{P}_{NL_j}\right)e^{-i\omega_j t} \tag{2.30}$$

Considering the electric field and the induced nonlinear polarization field, and assuming that spatially and temporally the amplitude changes very slowly, at least compared to the frequency of the plane wave, the following assumption can be made:

$$\frac{\partial^2\mathbf{E}_j}{\partial t^2} \;\ll\; \omega_j\frac{\partial\mathbf{E}_j}{\partial t} \;\ll\; \omega_j^2\mathbf{E}_j \tag{2.31}$$

$$\frac{\partial^2\mathbf{E}_j}{\partial z^2} \;\ll\; k_j\frac{\partial\mathbf{E}_j}{\partial z} \;\ll\; k_j^2\mathbf{E}_j \tag{2.32}$$

$$\frac{\partial^2\mathbf{P}_{NL_j}}{\partial t^2} \;\ll\; \omega_j\frac{\partial\mathbf{P}_{NL_j}}{\partial t} \;\ll\; \omega_j^2\mathbf{P}_{NL_j} \tag{2.33}$$

This assumption is known as the slowly varying envelope approximation (SVEA) [5]. The validity of the SVEA for the nonlinear polarization can be seen when considering the relative time scales. Light in the visible spectrum has a frequency of approximately $\omega_j \approx 10^{15}Hz$. The time it takes to polarize the medium is roughly $t_p \geq 10^{-12}s$.

This has the result that the second order spatial and temporal derivatives of the amplitude of the electric field and the first and second order temporal derivative of the nonlinear polarization can be neglected under the SVEA. Combining the nonlinear inhomogeneous wave equation (Equation 2.25) with Equations 2.28, 2.29 and 2.30, and taking these omissions into account, yields

$$\frac{1}{2}\sum_{j=1}^{N}\left(2ik_j\frac{\partial\mathbf{E}_j}{\partial z}-k_j^2\mathbf{E}_j-\frac{\epsilon_j}{c^2}\left[-2i\omega_j\frac{\partial\mathbf{E}_j}{\partial t}-\omega_j^2\mathbf{E}_j\right]\right)e^{i(k_jz)-\omega_jt} \;=\; \frac{1}{2}\frac{1}{c^2\epsilon_o}\sum_{j=1}^{N}\left(-\omega_j^2\mathbf{P}_{NL_j}\right)e^{i\omega_jt} \tag{2.34}$$

which can be further simplified by noting that $k_j^2=\frac{\epsilon_j\omega_j^2}{c^2}$. This yields

$$\sum_{j=1}^{N}\left(2ik_j\frac{\partial\mathbf{E}_j}{\partial z}+2i\frac{\epsilon_j}{c^2}\omega_j\frac{\partial\mathbf{E}_j}{\partial t}\right)e^{ik_jz} \;=\; \frac{-1}{c^2\epsilon_o}\sum_{j=1}^{N}\omega_j^2\mathbf{P}_{NL_j} \tag{2.35}$$

This holds true for each of the frequency components and thus, keeping in mind that $n_j=\sqrt{\epsilon_j}$ and $k_j=\frac{n_j\omega_j}{c}$, it follows that

$$\frac{\partial\mathbf{E}_j}{\partial z}+\frac{n_j}{c}\frac{\partial\mathbf{E}_j}{\partial t} \;=\; i\frac{\omega_j}{cn_j}\frac{1}{2\epsilon_o}\mathbf{P}_{NL_j}e^{ik_jz} \tag{2.36}$$

Equation 2.36 is then the well known, so-called nonlinear wave equation. It provides a framework for describing all the nonlinear light-matter interactions. Two such interactions, nonlinear refraction (self focussing) and nonlinear absorption, will be described in some detail.

2.2 Nonlinear Refraction (Self focusing)

Self focusing is a nonlinear process in which the beam that's passing through the nonlinear medium converges to a point as if it is passing through a converging lens, see figure 2.1. Since it is the fundamental laser beam that is influenced, it cannot be a three-wave interaction, but must be at least a four-wave interaction, as was shown in Section 2.1. In this analysis only a four-wave interaction will be considered since it is the dominant interaction in the case of self focusing [5]. This implies that the $\chi^{(2)}$ term in Equation 2.16 will play no part during self focusing and can thus be

neglected. Equation 2.16 will now read as follows

$$\mathbf{P(E)} = \epsilon_o(\chi^{(1)}\mathbf{E} + \chi^{(3)}\mathbf{E}^3 + \cdots) \tag{2.37}$$

which can be rewritten as

$$\mathbf{P(E)} = \frac{\epsilon_o}{2}(\chi^{(1)} + \chi^{(3)}|\mathbf{E}|^2 + \cdots)\mathbf{E} \tag{2.38}$$

Considering the term in the bracket to be the field-dependent susceptibility and disregarding the $\chi^{(4)}$ and higher terms, then analogously to the case of linear polarization (Equation 2.5), the nonlinear polarization can be written as

$$\mathbf{P(E)} = \frac{\epsilon_o}{2}\chi\left(|\mathbf{E}|^2\right)\mathbf{E} \tag{2.39}$$

with

$$\chi\left(|\mathbf{E}|^2\right) = \chi^{(1)} + \chi^{(3)}|\mathbf{E}|^2 \tag{2.40}$$

It was shown (Equation 2.18) that $\epsilon_1 = \chi^{(1)} + 1$. It is known that the linear index of refraction, n_0, relates to the dielectric constant through [5]

$$n_o = \sqrt{\epsilon_1} \tag{2.41}$$

for the case of negligible absorption, which implies that

$$n_o^2 = \chi^{(1)} + 1 \tag{2.42}$$

This implies that the refractive index, n, can analogously be written as

$$n^2 = 1 + \chi(|\mathbf{E}|^2) \tag{2.43}$$

and thus

$$n = \left(1 + \chi^{(1)} + \chi^{(3)}|\mathbf{E}|^2\right)^{\frac{1}{2}} \tag{2.44}$$

Using Equation 2.42 yields

$$n = \left(n_o^2 + \chi^{(3)}|\mathbf{E}|^2\right)^{\frac{1}{2}}$$

$$= n_o \left(1 + \frac{\chi^{(3)}|\mathbf{E}|^2}{n_o^2}\right)^{\frac{1}{2}}$$

$$\approx n_o + \frac{\chi^{(3)}|\mathbf{E}|^2}{2n_o^2} \equiv n_o + \frac{n_2}{2}|\mathbf{E}|^2 \tag{2.45}$$

and hence

$$n = n_o + n_2\langle\mathbf{E}\rangle = n_o + \triangle n \tag{2.46}$$

where n_2 being the nonlinear refractive index.
Self focusing can be easily understood, keeping in mind Equation 2.46, where it is shown that the refractive index is a function of the square of the electric field. This implies that the change in the refractive index (Δn) is a function of the intensity, $I(r)$.

$$\triangle n \propto I(r) \tag{2.47}$$

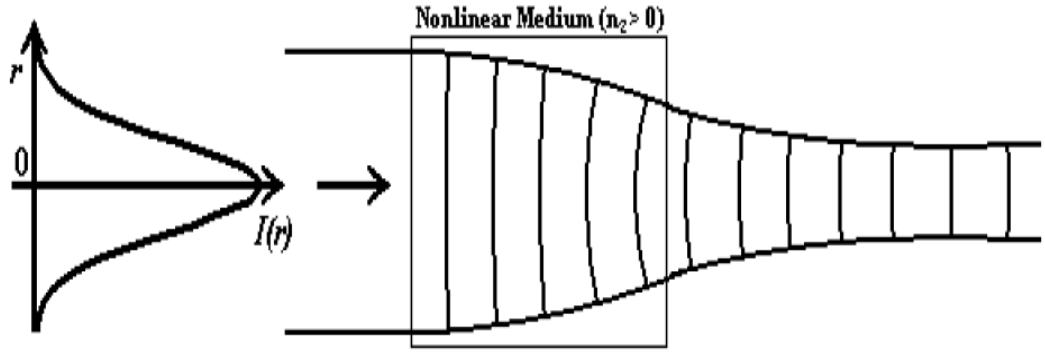

Figure 2.1: Self focusing of a Gaussian beam.

Considering incident laser light with a Gaussian intensity distribution, the intensity in the nonlinear material is higher in the center of the pulse than in the flanks of the pulse. The result is that the change in the refractive index of the material will be greater in the center of the pulse than in the flanks, which results in a greater

phase shift, $\Delta\phi(\Delta n)$, of the laser pulse in the center than in the flanks. The result is that the material will act as a lens. This effect is illustrated in Figure 2-1. The sign of the nonlinear index of refraction will determine whether focusing $(n_2 > 0)$ or defocusing $(n_2 < 0)$ will occur. Usually one distinguishes between weak self focusing and catastrophic self focusing, the difference being that in the first case the focus is outside the medium and in the second case it is within the medium.

2.2.1 Conditions for self focusing

To obtain an understanding of the conditions required for self focusing to occur, a summary of the discussion presented by Milonni and Eberly in their book "Lasers" [5] is given in this section. The wave equation for the electric field $(E = E_0 e^{-i\omega t})$, with the index of refraction given by Equation 2.46, is considered

$$\nabla^2\mathbf{E} - \frac{n^2}{c^2}\frac{\partial^2\mathbf{E}}{\partial t^2} \approx \nabla^2\mathbf{E} - \frac{1}{c^2}\left(n_o^2 + 2n_o n_2\mathbf{E}^2\right)\frac{\partial^2\mathbf{E}}{\partial t^2} = 0 \tag{2.48}$$

with the approximation that $n_2 \ll n_0$. In the paraxial approximation [5] and averaging over an optical period (which results in replacing $\mathbf{E}^2$ by $\frac{1}{2}|E_0|^2$) the result is

$$\nabla_T^2\mathbf{E}_o + 2ik\frac{\partial E_o}{\partial z} + \frac{k^2 n_2}{n_o}|E_o|^2 E_o = 0 \tag{2.49}$$

where $k = n_0\omega/c$ and $\nabla_T^2 = \frac{\partial^2}{\partial x^2} + \frac{\partial^2}{\partial y^2}$ is the transverse Laplacian. The $\nabla_T^2 E_0$ describes how the beam changes perpendicular to the propagation direction and thus the beam spreading (diffraction) that occurs. Since $\nabla_T^2 E_0$ describes how the beam changes perpendicular to the propagation direction; it is then dependent on the beam size or rather the beam cross section. In other words, beam spreading can be considered to be dependent on the beam cross section [5]. If the cross section is characterized by radius a_0, then

$$\nabla_T^2 E_o \sim a_o^{-2} E_o \tag{2.50}$$

The $\frac{k^2 n_2}{n_0}|E_0|^2 E_0$ term is the intensity dependent part which describes the self focusing. Self focusing can compete with diffraction if $\frac{k^2 n_2}{n_0}|E_0|^2 E_0$ is comparable to $\nabla_T^2 E_o$, that is if

$$\frac{k^2 n_2}{n_0}|E_0|^2 E_0 \sim a_o^{-2} E_o \tag{2.51}$$

or

$$a_o^2|E_o|^2 \sim \frac{n_0}{k^2 n_2} \tag{2.52}$$

The beam intensity (I) is related to the square of the electric field through $I = (n_0 c\epsilon_0/2)|E_0|^2$. The power ($P$) is related to the product of the intensity and the cross section of the beam. Using Equation 2.52 the critical beam power that is necessary to overcome the diffractive spreading of the beam is of the order

$$\begin{aligned} P_{cr} \sim (\pi a_o^2) I &= \frac{\pi n_o c\epsilon_o}{2} a_o^2 |E_o|^2 \\ &= \frac{\pi n_o c\epsilon_o}{2} \frac{n_o}{k^2 n_2} \\ &= \frac{\pi n_o^2 c\epsilon_o}{2k^2 n_2} \\ &= \frac{c\epsilon_o \lambda^2}{8\pi n_2} \end{aligned} \tag{2.53}$$

This approximation is in good agreement [5] with numerical integration of the nonlinear partial differential Equation 2.49. It can be seen that the beam power must exceeds a certain threshold for self focusing and not the beam intensity. A beam with power less than P_{cr} will not undergo self focusing even if it is focussed tighter [5]. The reason for this is that the diffractive spreading increases as the beam diameter is reduced, counteracting the self focusing.

When considering the processes that contribute to the optical limiting behavior of a material, the process that best attenuates a laser beam, and thus protects an optical sensor, is nonlinear absorption. The other processes namely the nonlinear refraction and nonlinear scattering are merely secondary in importance. This implies that when a material is identified as a possible optical limiter, it is the nonlinear absorption coefficient that will determine whether or not it will act as an effective optical limiter. To this end, it is necessary to construct a setup by means of which the nonlinear absorption coefficient can be measured.

2.3 Nonlinear Absorption

Linear absorption phenomena can be described according to Beer's law which state that

$$I = I_o e^{-\alpha(\omega)z} \tag{2.54}$$

where I_o is the incident intensity, $\alpha(\omega)$ is the linear absorption coefficient, z is the propagation depth in the absorbing medium and $I(z)$ is the intensity at depth z. Beer's law is merely the solution of the differential equation that describes how light intensity decreases with propagation depth (z) in a medium for the case where α is a constant

$$\frac{\partial I}{\partial z} = -\alpha(\omega)I \tag{2.55}$$

If nonlinear (multi-photon) effects are to be included then this differential equation must be extended to include higher order intensity terms [8],

$$\frac{\partial I}{\partial z} = -\alpha(\omega)I - \beta(\omega)I^2 - \gamma(\omega)I^3 - O(\omega)I^4 \tag{2.56}$$

where $\beta(\omega)$ is the two-photon absorption coefficient, $\gamma(\omega)$ is the three-photon absorption coefficient and $O(\omega)$ represents the four-photon absorption term.

If a material displays negligible linear absorption and two-photon absorption dominates, then only the second term on the right of Equation 2.56 needs to be considered and the other terms can be disregarded. This implies that only

$$\frac{\partial I}{\partial z} = -\beta(\omega)I^2 \tag{2.57}$$

needs to be solved. This can be done by separation of variables [7] which yields

$$I(z) \; = \; \frac{I_o}{1 + \beta I_o z} \tag{2.58}$$

where I_0 is again the incident intensity, β the two-photon absorption coefficient and z the distance that the light has travelled in the sample. It can clearly be seen from equation 2.58 that two-photon absorption results in much stronger absorption and thus more beam attenuation. This is as a result of the intensity dependent nature

of nonlinear absorption.

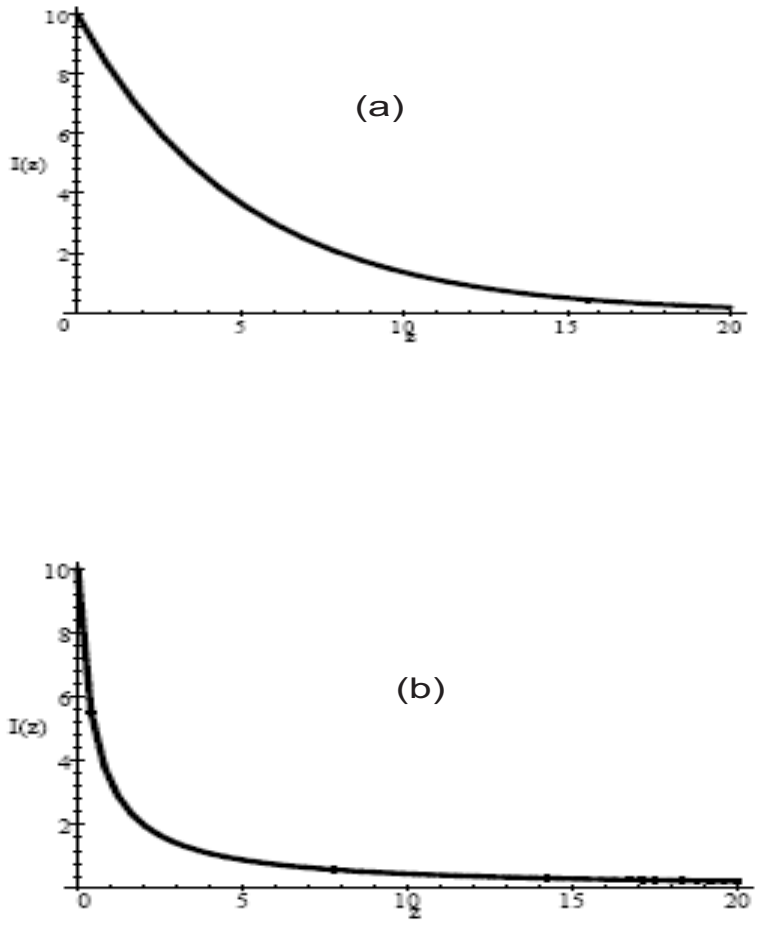

Figure 2.2: A schematic graph depicting (a) linear absorption (I_o=10, α=0.2) and (b) pure two-photon absorption (I_o=10, β=0.2), z being the depth in the sample.

Chapter 3

Z-scan

The Z-scan works on the principle of moving the sample under investigation through the focus of a tightly focussed Gaussian laser beam. The interaction of the medium with the laser light changes as the sample is moved. This is because the sample experiences different intensities, dependent on the sample position (z) relative to the focus ($z = 0$). By measuring the transmitted power (the transmittance) through the sample as a function of z-position of the sample, information about the light-matter interaction can be extracted. The two nonlinear interactions that can be determined in this fashion are the samples nonlinear index of refraction and nonlinear absorption coefficient. For the measurement of the nonlinear index of refraction an aperture is placed in front of the detector measuring the transmitted light. This makes the measurement sensitive to the beam spreading or focusing and relates to a transformation of phase distortion into amplitude distortion.

3.1 Z-Scan Theory

In this section a theoretical background for analyzing the Z-Scan technique is formulated [9]. In general, for the case of cubic nonlinearity, the index of refraction(n) is expressed in terms of nonlinear indices $n_2(esu)$ or $\gamma(m^2/W)$ through

$$n = n_o + \frac{n_2^2}{2}|E^2| = n_o + \gamma I = n_o + \Delta n(I) \tag{3.1}$$

Where n_o is the linear index of refraction, E is the peak electric field (cgs), and I

denotes the irradiance (MKS) of the laser beam within the sample. The n_2 and γ are related through the conversion formula $n_2(esu) = (cn_o/40\pi)\gamma(m^2/W)$, where c(m/s) is the speed of light in vacuum. Assuming a Gaussian beam of light waist radius w_o travelling in +z direction, we can write E as

$$E(z,r,t) \;=\; E_o(t)\frac{w_o}{w(z)}e^{\;-\frac{r^2}{w^2(z)}-\frac{ikr^2}{2R(z)}}\;\; e^{-i\phi(z,t)} \tag{3.2}$$

where $w^2(z) = w_o^2(1+\frac{z^2}{z_o^2})$ is the beam radius, $R(z) = z(1+\frac{z_o^2}{z^2})$ is the radius of curvature of the wavefront at z, $z_0 = kw_o^2/2$ is the diffraction length, i.e., the Reyleigh Distance of the beam, $k = 2\ \pi/\lambda$ is the wave number, and λ is the wavelength of the laser, all in free space. E_o(t) is the radiation electric field at the focus and contains the temporal envelope of the laser pulse. The co-ordinate axis used for the Z-scan theoretical analysis are depicted in Fig. 3.1. The $e^{-i\phi(z,t)}$ term contains all the radially uniform phase variations. Since we are only concerned with calculating the radial phase variation $\Delta\phi(r)$, the slowly varying envelope approximation (SVEA) [10] applies, and all other phase changes that are uniform in r are ignored.

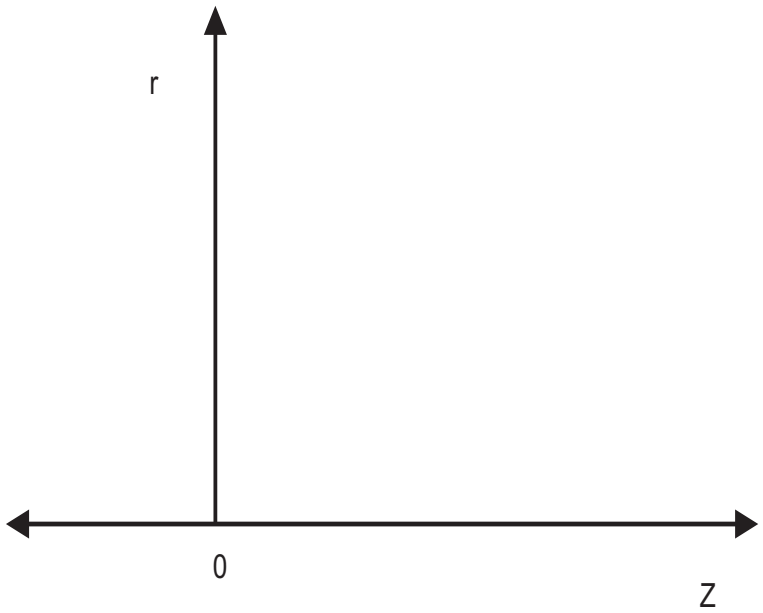

Figure 3.1: Co-ordinate axis configuration for Z-Scan analysis

If the sample length is small enough that changes in beam diameter within the sample due to either diffraction or nonlinear refraction can be neglected, then we may regard this medium as "thin", in which case self refraction is regarded as "external self action". For linear refraction, this implies that $L \ll z_o$, and for nonlinear refraction, $L \ll z_o/\Delta\phi(0)$[11]. In most of the Z-Scan experiments the second critical condition is automatically met since $\Delta\phi$ is small. It is also found that first criterion can be made less restrictive to $L < Z_o$ [10]. This assumption simplifies the problem considerably, and the amplitude $\sqrt{I}$ and ϕ of the electric field as a function of z′ are governed by SVEA by a pair of simple equations:

$$\frac{d\Delta\phi}{dz'} \;=\; \Delta n(I)k \tag{3.3}$$

and

$$\frac{dI}{dz'} \;=\; -\alpha(I)I \tag{3.4}$$

Where z′ is the propagation depth in the sample and $\alpha(I)$, in general includes linear and nonlinear absorption terms. Note that z′ should not be confused with the sample position z. In the case of cubic nonlinearity, Eq. (3.3) and (3.4) are solved to get the phase shift $\Delta\phi$ at the exit surface of the sample which follows the radial variation of the incident irradiance at a given position of the sample z. Thus,

$$\Delta\phi(z,r,t) \;=\; \Delta\phi_o(z,t)exp\left(-\frac{2r^2}{w^2(z)}\right) \tag{3.5}$$

with

$$\Delta\phi(z,t) \;=\; \frac{\Delta\phi_o(t)}{1+\frac{z^2}{z_o^2}} \tag{3.6}$$

Where $\Delta\phi_o(t)$, is on axis phase shift at the focus, and is defined as

$$\Delta\phi_o(t) \;=\; k\Delta n_o(t)L_{eff}$$

Where

$$L_{eff} \;=\; (1-e^{-\alpha L})/\alpha \tag{3.7}$$

with L the sample length and α the linear absorption coefficient. Here $\Delta n_o = \gamma I_o(t)$

with $I_0(t)$ being on axis irradiance at the focus (i.e. $z = 0$). We ignored Fresnel reflection losses, for example $I_0(t)$ is the irradiance with in the sample.

The complex electric field exiting the sample E, now contains the nonlinear phase distortion

$$E_e(z, r, t) \;=\; E(z, r, t)e^{-\alpha L/2}e^{i\Delta\phi(z,r,t)} \tag{3.8}$$

From the Huygen's principle, one can obtain the far field pattern of the beam at the aperture plane through a Zeroth-order Henkel transformation of E_e. we follow a method called "Gaussian Decomposition" [11] which is more suitable for Gaussian beams. In this method, we decompose the complex electric field at the exit plane of the sample into a summation of Gaussian beams through a Taylor series expansion of the nonlinear phase term $e^{i\Delta\phi(z,r,t)}$ in Eq.(3.8). That is

$$e^{i\Delta\phi(z,r,t)} \;=\; \sum_{m=0}^{\infty} \frac{[i\Delta\phi_o(z,t)]^m}{m!} e^{-2mr^2/w^2(z)} \tag{3.9}$$

Each Gaussian beam now propagates to the aperture plane where it will contribute to reconstruct the beam. We write the resultant electric field pattern at the aperture as

$$E_a(r, t) \;=\; E(z, r = 0, t)e^{-\alpha L/2} \sum_{m=0}^{\infty} \frac{[i\Delta\phi_o(z,t)]^m}{m!} \frac{w_{mo}}{w_m} exp\left(-\frac{r^2}{w_m^2} - \frac{ikr^2}{2R_m} + i\theta_m\right) \tag{3.10}$$

Defining d_1 as the propagation distance in free space from the sample to the aperture plane and $g = 1 + d_1/R(z)$ the remaining parameters in Eq.(3.10) are expressed as

$$w_{mo}^2 \;=\; \frac{w^2(z)}{2m+1}$$

$$d_m \;=\; \frac{kw_{mo}^2}{2}$$

$$w_m^2 \;=\; w_{mo}^2\left[g^2 + \frac{d_1^2}{d_m^2}\right]$$

$$R_m \;=\; d\left[1 - \frac{g}{g^2 + \frac{d_1^2}{d_m^2}}\right]^{-1}$$

$$\theta_m \;=\; \tan^{-1}\left[\frac{d_1/d_m}{g}\right]$$

The expression given by Eq.(3.10) is a general case derived by Weaire where by the collimated beam of $R = 0$ is considered for which $g = 1$.

The transmitted power through the aperture is obtained by spatially integrating $E_a(r,t)$ up to the aperture radius r_a, giving

$$P_T(\Delta\phi_o(t)) \;=\; c\varepsilon_o n_o \pi \int_0^{r_a} |E_a(r,t)|^2 r dr \tag{3.11}$$

where ε_o is the permittivity of vacuum. Including the pulse temporal variation, the normalized Z-Scan transmittance T(z) can be calculated as

$$T(z) \;=\; \frac{\int_{-\infty}^{\infty} P_T(\Delta\phi_o(t))dt}{S\int_{-\infty}^{\infty} P_i(t)dt} \tag{3.12}$$

Where $P_i(t) = \pi w_o^2 I_o(t)/2$ is the instantaneous input power with in the sample and $S = 1 - exp(-2r_a^2/w_a^2)$ is the aperture linear transmittance, w_a denoting the beam radius at the aperture in the linear regime.

For the cubic nonlinearity and a small phase change the on-axis Z-Scan transmittance can be obtained by letting $r = 0$ in Eq.(3.10). Also due to small phase change i.e. $|\Delta\phi| \ll 1$, only two terms in Eq.(3.10) are retained. One arrives at the normalized Z-Scan transmittance as given by

$$\begin{aligned} T(z,\Delta\phi) \;&=\; \frac{|E_a(z,r=0,\Delta\phi_o)|^2}{|E_a(z,r=0,\Delta\phi_o=0)|^2} \\ &=\; \frac{|(g+id/d_o)^{-1} + i\Delta\phi_o(g+id/d_1)^{-1}|^2}{|(g+id/d_o)^{-1}|^2} \end{aligned} \tag{3.13}$$

The far field condition d_o, can be further simplify Eq.(3.13) to get the geometry independent normalized transmittance as

$$T(z,\Delta\phi_o) \;\approx\; 1 - \frac{4\Delta\phi_o x}{(x^2+9)(x^2+1)} \tag{3.14}$$

Where $x = z/z_o$.

The Z-Scan theory described above can be extended to include the nonlinear absorption effects in the nonlinear sample. To develop this theory, we analyze two-photon absorption (2PA), in semiconductor with $E_g < 2h\omega < 2E_g$, where E_g is the bandgap energy and ω is the optical frequency. The third order nonlinear susceptibility is considered to be a complex quantity, given by,

$$\chi^{(3)} = \chi_R^{(3)} + i\chi_I^{(3)} \tag{3.15}$$

The imaginary part is related to the 2PA coefficient through

$$\chi_I^{(3)} = \frac{n_o^2 \varepsilon_o c^2}{\omega}\beta \tag{3.16}$$

and real part is related to γ through

$$\chi_R^{(3)} = 2n_o^2 \varepsilon_o c\gamma \tag{3.17}$$

We neglected the free-carrier effects as we are concerned with low excitation regime. In view of this approximation we write:

$$\alpha(I) = \alpha + \beta I \tag{3.18}$$

This yields the irradiance distribution and phase shift of the beam at the exit surface of the sample as

$$I_e(z,r,t) = \frac{I(z,r,t)e^{-\alpha L}}{1+q(z,r,t)} \tag{3.19}$$

and

$$\Delta\phi(z,r,t) = \frac{k\gamma}{\beta}\ln[1+q(z,r,t)] \tag{3.20}$$

Where $q(z,r,t) = \beta I(z,r,t)L_{eff}$. Combining Eq.(3.19) and (3.20), we obtain the complex field at the exit surface of the sample as

$$E_e = E(z,r,t)e^{-\alpha L/2}(1+q)^{(ik\gamma/\beta - 1/2)} \tag{3.21}$$

Above equation reduces to Eq.(3.8) in the limit of no two photon absorption. A zeroth

order Henkel transform of Eq.(3.21) gives the field distribution at the aperture which then can be used in Eq.(3.11) and (3.12) to yield the transmittance. For $|q|$, following a binomial series expansion in powers of q, Eq.(3.21) can be expressed as an infinite sum of Gaussian beams similar to the purely refractive case described earlier as follows:

$$E_e \;=\; E(z,r,t)e^{-\alpha L/2}\sum_{m=0}^{\infty}\frac{q^m(z,r,t)}{m!}\left[\prod_{n=0}(ik\gamma/\beta-1/2-n+1)\right] \tag{3.22}$$

Where Gaussian spatial profiles are implicit in Eq.(3.10). The result is represented by Eq.(3.10) if we substitute the $(i\Delta\phi_o(z,t))^m/m!$ terms in the sum by

$$f_m \;=\; \frac{(i\Delta\phi_o(z,t))^m}{m!}\prod_{n=0}^{m}\left(1+i(2n-1)\frac{\beta}{2k\gamma}\right) \tag{3.23}$$

With $f_o = 1$. Note that the coupling factor $\beta/2k\gamma$ is the ratio of the imaginary to real part of the third order nonlinear susceptibility, $\chi^{(3)}$.

As evident from Eq.(3.23), the absorptive and refractive contributions in the far field beam profile and hence open and closed aperture Z-Scan transmitted is only a function of nonlinear absorption. The total transmitted fluence in the open aperture case can be calculated by spatially integrating Eq.(3.19) with out having to include the free space propagation process. Integrating Eq.(3.19) at z over r, we obtain the transmitted power $P(z,t)$ as follows:

$$P(z,t) \;=\; P_i(t)e^{-\alpha L}\frac{\ln[1+q_o(z,t)]}{q_o(z,t)} \tag{3.24}$$

Where $q_o(z,t) = \frac{\beta I_o(t)L_{eff}}{1+z^2/z_o^2}$ and $P_i(t)$ is defined in Eq.(3.12). For a temporally Gaussian pulse above equation can be integrating to give the normalized energy transmittance

$$T(z,S=1) \;=\; \frac{1}{\sqrt{\pi}q_o(z,0)}\int_{-\infty}^{\infty}\ln[1+q_o(z,0)e^{-\tau^2}]d\tau \tag{3.25}$$

For $|q_o| < 1$, this transmittance can be expressed in terms of peak irradiance in a summation form more suitable for numerical evaluation:

$$T(z,S=1) \;=\; \sum_{m=0}^{\infty}\frac{[-q(z,0)]^m}{(m+1)^{3/2}} \tag{3.26}$$

Thus once the open aperture Z-Scan is performed, nonlinear absorption coefficient β can be determined. Usually a simplified form of the above Eq.(3.26) is used by considering only first two terms of the summation and is given by

$$T(z, S = 1) \; = \; 1 - \frac{\beta I_o(t) L_{eff}}{(1 + \frac{z^2}{z_o^2}) 2^{3/2}} \tag{3.27}$$

3.2 Z-Scan Technique

There are numerous techniques for measuring the nonlinear index of refraction and the nonlinear absorption coefficient of materials. The Z-scan is amongst the simplest and most sensitive techniques. The basic Z-scan technique has been described by Mansoor Sheik-Bahae et al [10, 12].

Z-Scan technique can be described as measuring the transmittance of a nonlinear medium as a function of the sample position(z) measured with respect to focal plane. In the following paragraphs we explain in detail how such a trace is related to nonlinear refraction of the sample.

To understand the Z-Scan[13], let's assume that the nonlinear index of the thin film under test is positive, and the sample is in prefocal position as shown in Fig. 3.2. The Kerr type nonlinear thin film may be viewed as a lens if we assume that the response the film follows the transverse light profile. In the far field the beam opens up more owing to combined diffraction from the nonlinear lens and focussing lens. It remains collimated over shorter distance in the near field; and diverges at larger beam angle in the far field correspondingly reducing irradiance at the detector. When the same sample passes through the focal point to postfocal point position, the positive lensing of the nonlinear thin film tends to reduce beam divergence, which in turn results in increased irradiance at the detector in the far field. Hence one would observe a characteristic valley and peak in transmission spectra when a positive index nonlinear material is scanned from prefocal to postfocal region. The situation is reversed if negatively nonlinear index thinfilm is under Z-Scan test. The characteristics of the scan are peak and valley as the sample is scanned. In open aperture Z-Scan,

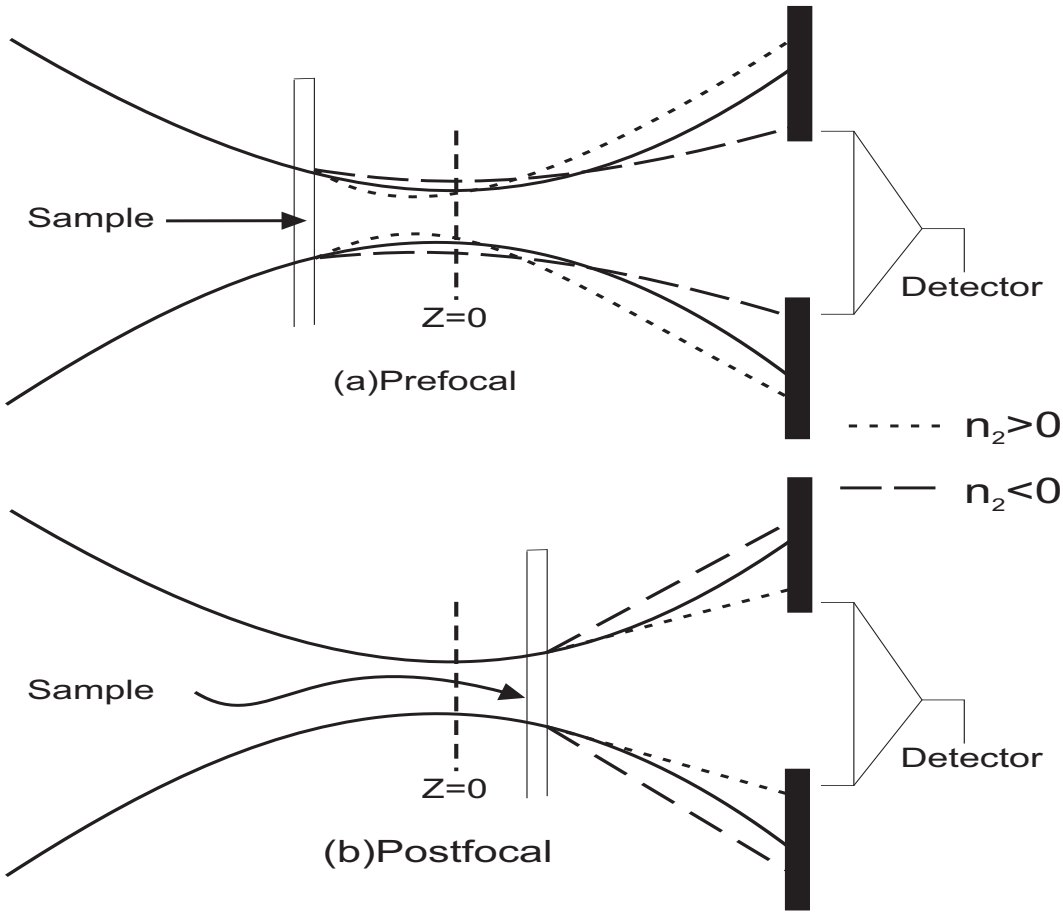

Figure 3.2: Nonlinear refraction measurement through Z-Scan method (dark lines denote beam propagation without nonlinear sample in the path).

we collect the entire light output from the sample. This yields the information on its nonlinear absorption properties. While in the close aperture experiment, we limit the detector reading to light propagating along the 'z' axis. This yields the information about the nonlinear refraction of the sample.

3.3 Z-Scan Experimental Setup

The basic experimental setup for Z-scan measurement can be seen in Figure 3.3. In the figure, BS is a beam-splitter, D1 is the reference detector, D2 the probe detector and the sample is at position z. An aperture is placed in front of the probe detector

when measuring the nonlinear index of refraction.

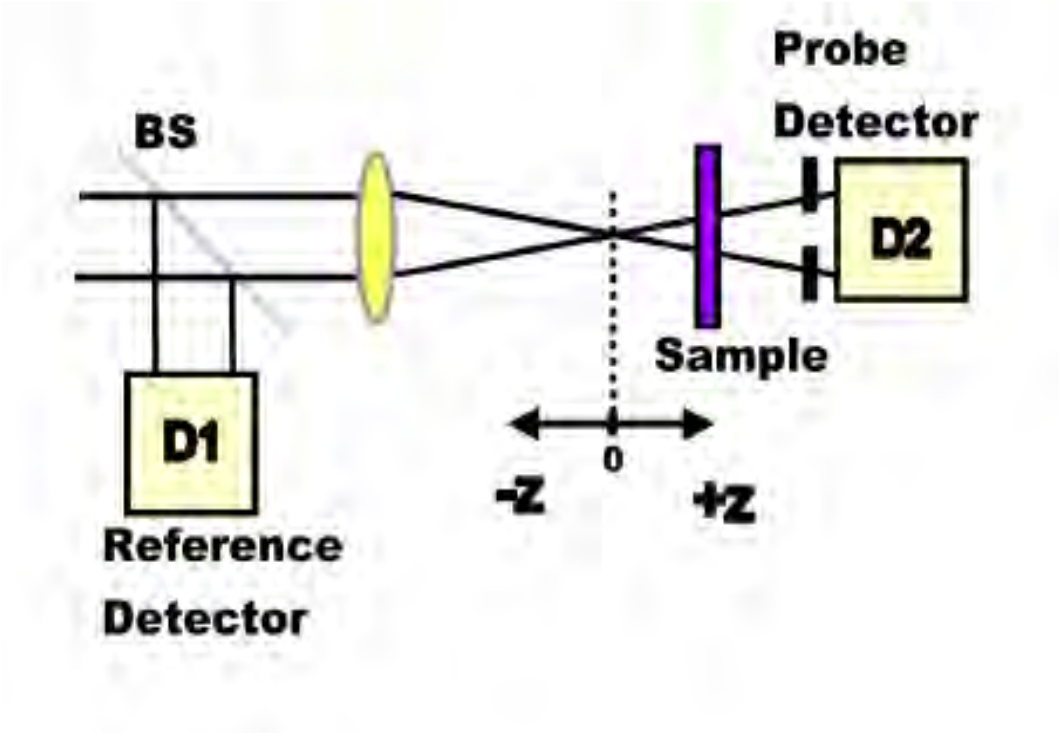

Figure 3.3: The basic Z-Scan setup.

A sample displaying nonlinear refraction will act as a lens of variable focal length as it is moved along the z-axis. An example of this is the following: Consider a material with a negative nonlinear index of refraction and a thickness less than the diffraction length (also known as the Rayleigh length, z_o) of the focussed laser beam. The sample exhibits negligible nonlinear refraction when it is far from the focus, because of the low intensity of the laser beam at this position. As the sample is moved towards the focus; it starts acting as a negative lens (collimating the beam and shifting the waist of the laser beam). The result is a smaller spot size at the aperture placed in front of the detector, and thus a higher transmittance through the aperture (see Figure 3.3). This effect increases as the sample is moved towards the focus due to the intensity increase. A maximum transmittance through the aperture will occur when the sample is just in front of the focus. This maximum in transmittance (peak) will

drop to a minimum (valley) as the sample is moved further and the beam diverges as a result of the negative lensing by the sample. The transmittance through the aperture will again return to the linear value as the sample is moved further from the focus. The result of a scan such as this is a transmittance versus position graph which has a peak followed by a valley. When the sample has a positive nonlinear index of refraction then the graph is inverted.

Chapter 4

Experiment

In the present investigation five different types of artificial Porphyrins: Zinc Meso-Tetraphenyl Porphine (ZnTPP); 5,10,15,20-Tetraphenyl 21H, 23H-Porphine Copper (II) (CuTPP); Vanadium (IV) Oxide Meso-Tetraphenyl Porphine (VaTPP); Palladium (II) 2,4-Pentanedionate (PaPD) and Manganese (III) Acetate Meso-Tetraphenyl Porphine (MnTPP) are used. The samples were prepared from Toluene based Porphyrin solutions at concentrations ranging from $10^{-6}M$ up to $4 * 10^{-3}M$. The Nafion membranes were first cut to sizes of 8mm X 8mm. The membranes were then rinsed in to warm concentrated Nitric acid for 30 minutes to remove inorganic impurities, followed by cleaning with warm ($50^{0}c$) Toluene. The cleaned membranes were immersed into the Porphyrin solutions and kept for an average of 16 hours in a warm oven. Finally, the membranes were dried at room temperature and kept between thin transparent glass plates for further investigation.

4.1 Absorption Spectrum Measurement

The instrument which is used to measure the absorption spectrum of the samples is Cary 1E UV-Visible . This measurement is done in two types of samples, one in solution form (Porphyrins dissolved in Toluene) and the other in solid form (Porphyrins incorporated in Nafion membrane) for each of the five Porphyrins. Shifts of the absorption peaks of the Porphyrins in Nafion as compared to the Porphyrins in

Toluene solvent are expected which exists due to the reaction of Nafion with the Porphyrins. This shifts are the confirmation that the samples are successfully prepared (Porphyrins are successfully embedded with in the holes of the membrane). The shifts of the peaks increases as the amount of Porphyrins with in the hole of the membrane increases up until it reaches some saturation value. The absorption measurement is also used to determine the wave length of the light source for which the Porphyrins can be an optical limiter. That is the type of laser source that is going to be used for the Z-Scan measurement is nominated from the absorption spectrum of the samples. The absorption at this wave length must be very weak since the intensity of the light source in the spectrophotometer is insufficient to cause nonlinear effect. The other very important use of the absorption measurement is to check the degradation of the samples. Degradation in this context is to mean the undesired reaction of the Porphyrins with the environment and end up with being something else. The degradation is expected to bring about a change on the absorption spectrum of the materials.

4.2 Z-Scan Measurement

The open aperture Z-Scan measurement employed here is the Nd:Yag laser (1064nm, 10ns) in its second harmonic mode (532nm) with a lens of focal length 62.9mm (See figure.3.3). The wave length of the laser source is chosen to be 532nm because at this wave length the absorption of the Porphyrins is very weak as shown in figure.5.1. The convex lens make the laser beam to have a Gaussian type of intensity profile which gives the sample that's moving along the Z-axis a chance to experience different intensities of light. Since the sample is expected to show nonlinear effect, it start absorbing the light when its intensity is high (around the focal point of the lens). At the focal point, the intensity is so high that almost all of the light is absorbed. As we move away from the focal point the intensity of the laser decreases so as the absorption. Due to the fact that the Gaussian like intensity profile of the laser source is symmetric about the focal point along the Z-axis, a symmetrical absorption profile about the focal point is expected. This symmetrical nonlinear absorption is observed as a valley around the focal point, see figure.5.2.

Chapter 5

Results and Discussion

5.1 Absorption Spectrum Result

The optical absorption spectra of all the Porphyrins were measured in the form of solution as well as after they are incorporated within Nafion membrane. The absorption spectra of ZnTPP as shown in Figure.5.1(a), distinctly showed two peaks at 422nm and 548nm wavelengths which represents the Soret and Q-band peaks, respectively. These peaks are redshifted due to the incorporation of the Porphyrin in Nafion membrane. The Soret band peak shifted from 422nm to 434nm while the Q-band peak shifted from 548nm to 653nm. The observed redshifts are in agreement with previously reported experimental results. The red shifts are attributed to the reaction of Nafion with that of the incorporated Porphyrin compounds [14, 15]. Similar redshifts are observed for VaTPP as shown in Figures.5.1(B). The shifts in the case of VaTPP are from 423nm to 430nm and from 547nm to 652nm for Soret and Q-band peaks respectively. Further more CuTPP also showed similar shifts as ZnTPP and VaTPP. As its Soret band shifts from 417nm to 435nm, its Q-band shifts from 539nm to 652nm. However, the spectra taken from MnTPP and PaPD that are confined in Nafion membrane did not show any sign of the redshift that probably indicate no metal ions and proton exchange reaction took place with these Porphyrins.

In general, the absorption spectrum profiles of the Porphyrins in Nafion membrane showed an increment in absorbance at the peaks and broadening of the Soret

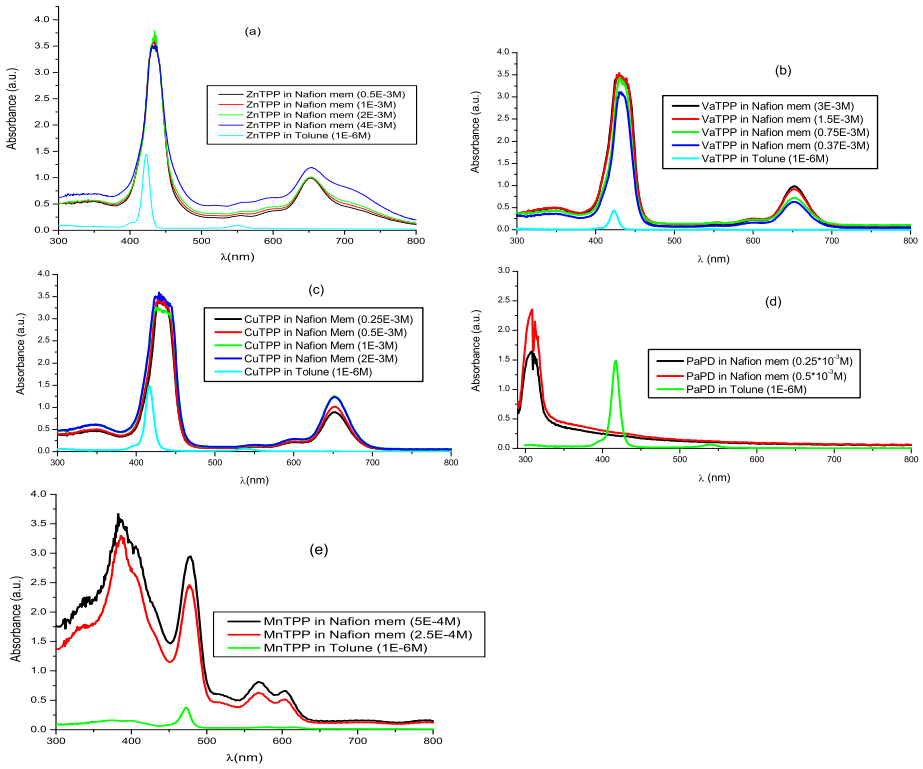

Figure 5.1: The UV-Visible absorption spectrum of (a) ZnTPP, (b) VaTPP, (c) CuTPP, (d) PaPD and (e) MnTPP.

and Q-bands when they are compared with their corresponding results in their solution form. The lifting up of the peaks is due to the high concentration of the porphyrin solutions in which the membranes were kept for 16 hours during their incorporation. As it can be seen in figure 5.1 the absorbance value at the peaks increases with the concentration of the solutions. The broadening of the bands could be due to the reaction of the membrane with the Porphyrins which results to the replacement of the metal ions in the Porphyrins with protons to form free base Porphyrins [15].

Porphyrins in the solution form is known to undergo degradation when exposed to the environment [16]. Where as Porphyrins in Nafion membrane are safe from

environmental degradation. In this study the stability of Porphyrins in Nafion matrix is studied by comparing the absorption spectrum of fresh samples and the same samples after exposing them to the environment for 30 days. Both of the spectrum are the same which confirms the stability of Porphyrins which are incorporated in Nafion membrane.

5.2 Z-Scan Result

Open aperture Z-scan measurements show the nonlinear absorption and optical limiting behaviors of the materials. The Z-scan measurement data taken from pure Nafion membrane has no nonlinear optical property of its own. However, those membranes containing the Porphyrins did show the nonlinear characteristics which can be seen from the valley around the focus of the lens ($Z = 0$), as shown in Figure 5.2. So, the creation of the valley around the focus where the intensity of the laser is very high shows intensity dependent (nonlinear) absorption which is attributed for the Porphyrins incorporated with in Nafion membrane. Using the Z-Scan theory and fitting the Z-Scan data with Eq.(3.27); the nonlinear absorption coefficient (β) for each of the samples is determined.

Nonlinear absorption occurs when the intensity of the laser source is large enough which occurs around the focus of the lens ($z = 0$). Around this point Beer's law of linear absorption (see section 2.3) can not be applied to determine the linear absorption coefficient ($\alpha(\lambda)$) of the material. Beer's law can be applied at point where the intensity of the laser source is relatively low. These points are found at the flanks of the Z-Scan data (around $z = \pm 12mm$). By measuring the intensities of the laser source with (I) and with out the sample (I_0) at these points and using Eq. 2.54 the linear absorption coefficient of the Porphyrins is determined.

Figure 5.3 show the open aperture Z-Scan traces for ZnTPP incorporated in Nafion with its theoretical fit. The data is fitted with Eq. (3.27) using Origin programming software package. From the fit the nonlinear absorption coefficients (β) are determined as shown in table 5.1 with their linear absorption coefficient. As was previously

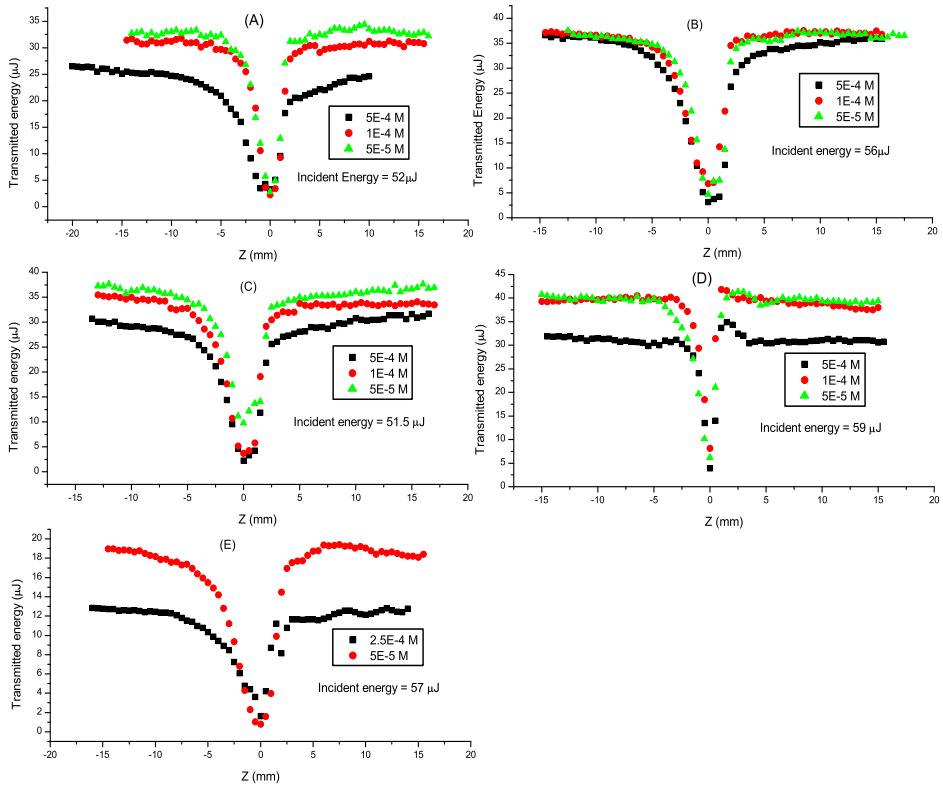

Figure 5.2: Open aperture Z-Scan traces of (a) ZnTPP, (b) VaTPP, (c) CuTPP, (d) PaPD, (e) MnTPP as they are incorporated in Nafion membrane.

reported by other results on different materials [4, 17], the value of β increases with the amount of Porphyrins incorporated (concentration of Porphyrin solution). That is the higher the concentration, the larger the value of β provided that all conditions are controlled.

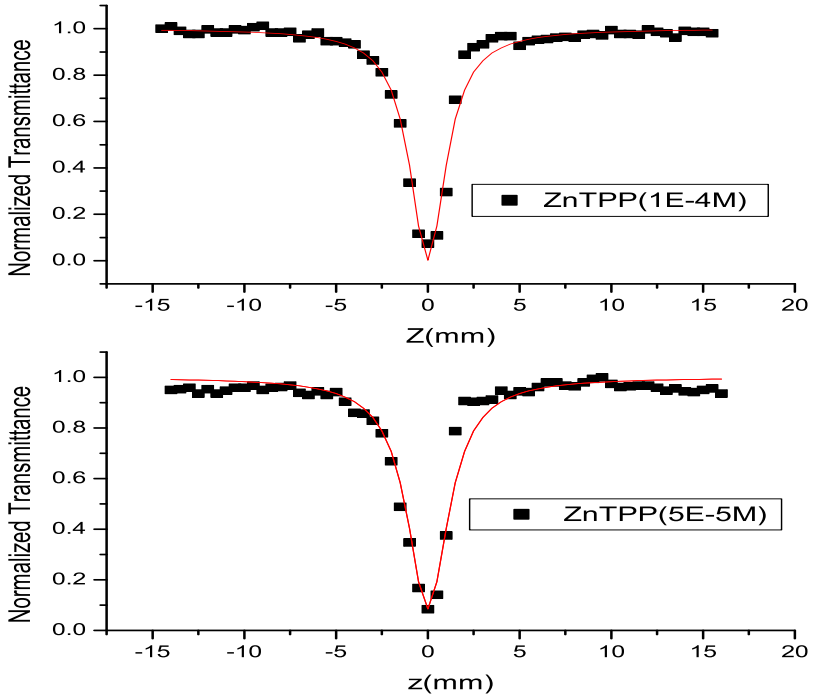

Figure 5.3: Z-scan of ZnTPP in Nafion along with the fitted function (solid line) on the data for concentrations of (a)1*10^{-4}M and (b)5*10^{-5}M

Table 5.1: Linear and nonlinear absorption coefficients of ZnTPP with their theoretical fitting errors.

Data	$\beta(\frac{cm}{MW})$	Fitting error			$\alpha(mm^{-1})$
		$\Delta\beta$	% error	χ^2	
ZnTPP(5E-4M)	0.25719	0.0084	3.27	0.90435	4.48
ZnTPP(1E-4M)	0.176	0.00293	2.7	0.94184	
ZnTPP(5E-5M)	0.149	0.00457	1.9	0.97102	

The linear and nonlinear absorption coefficient results of CuTPP obtained from figure 5.4 is summarized in table 5.2.

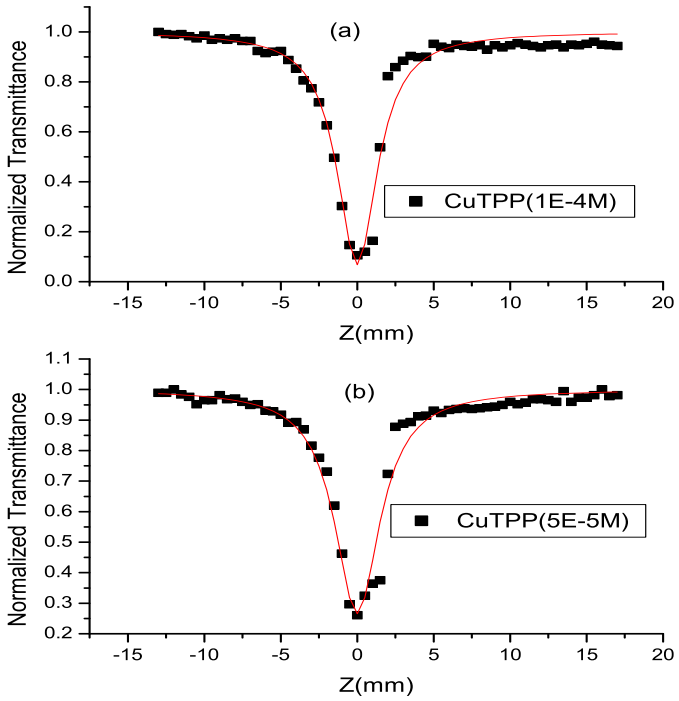

Figure 5.4: Z-scan of CuTPP in Nafion along with the fitted function (solid line) on the data for concentrations of (a)1*10^{-4}M and (b)5*10^{-5}M

Table 5.2: Linear and nonlinear absorption coefficients of CuTPP with their theoretical fitting errors.

Data	$\beta(\frac{cm}{MW})$	Fitting error			$\alpha(mm^{-1})$
		$\Delta\beta$	% error	χ^2	
CuTPP(5E-4M)	0.21104	0.00401	1.9	0.96649	3.22
CuTPP(1E-4M)	0.1763	0.00392	2.1	0.95861	
CuTPP(5E-5M)	0.14862	0.00333	2.1	0.95723	

The linear and nonlinear absorption coefficients for the different concentrations of VaTPP is determined in a similar fashion as was followed for ZnTPP and CuTPP above. The values are stated in table 5.3 which are obtained from figure 5.5. As was described above the values of β increases with the increases in concentrations.

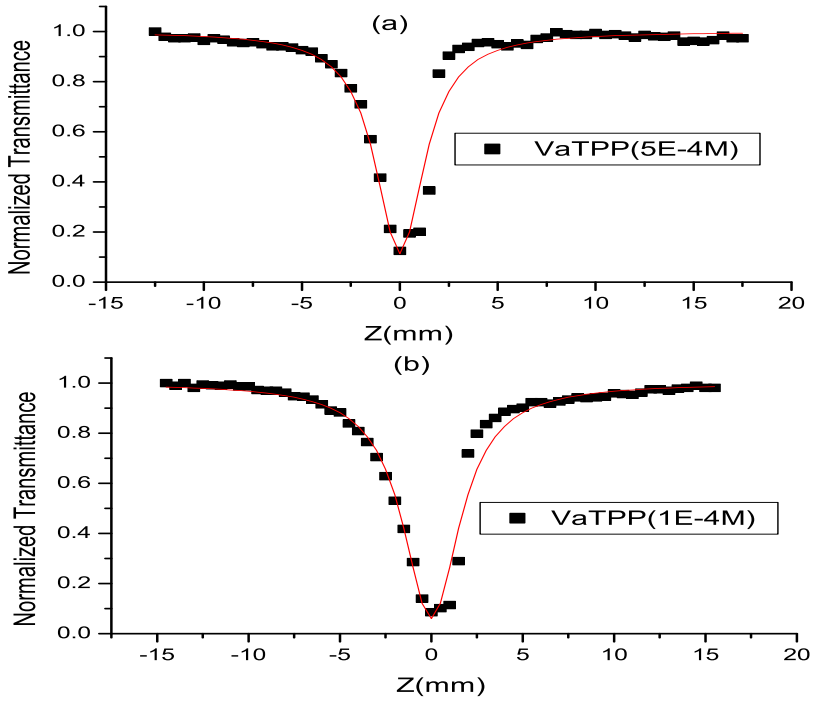

Figure 5.5: Z-scan of VaTPP in Nafion along with the fitted function (solid line) on the data for concentrations of (a)5*10^{-4}M and (b)1*10^{-4}M

Table 5.3: Linear and nonlinear absorption coefficients of VaTPP with their theoretical fitting errors.

Data	$\beta(\frac{cm}{MW})$	Fitting error			$\alpha(mm^{-1})$
		$\Delta\beta$	% error	χ^2	
VaTPP(5E-4M)	0.19853	0.00383	1.9	0.9489	2.5
VaTPP(1E-4M)	0.17302	0.00337	1.9	0.96795	
VaTPP(5E-5M)	0.16237	0.00521	3.2	0.92352	

Table 5.4 show linear and nonlinear absorption coefficients for different concentrations of PaPD including the theoretical fitting errors. These values are extracted

from figure 5.6.

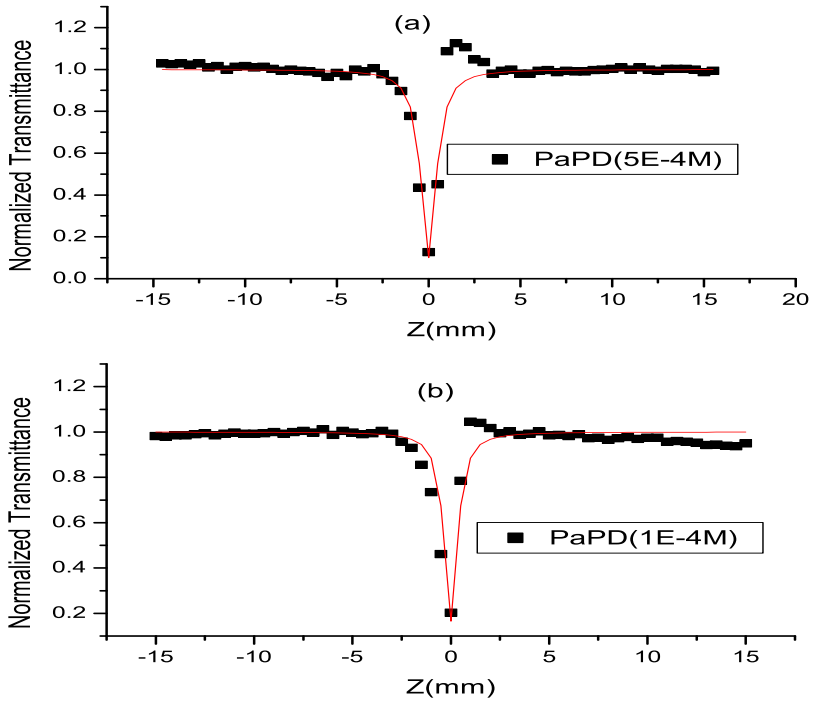

Figure 5.6: Z-scan of PaPD in Nafion along with the fitted function (solid line) on the data for concentrations of (a)5*10^{-4}M and (b)10^{-4}M.

Table 5.4: Linear and nonlinear absorption coefficients of PaPD with their theoretical fitting errors.

Data	$\beta(\frac{cm}{MW})$	Fitting error			$\alpha(mm^{-1})$
		$\Delta\beta$	% error	χ^2	
PaPD(5E-4M)	0.06313	0.0031	4.9	0.85567	3.37
PaPD(1E-4M)	0.04955	0.00243	4.9	0.86784	
PaPD(5E-5M)	0.03415	0.00181	5.3	0.83502	

Similar determinations of linear and nonlinear absorption coefficients for the Porphyrin MnTPP is carried out and the results are displayed in table 5.5. Figure 5.7 shows the Z-scan results with their theoretical fits for MnTPP.

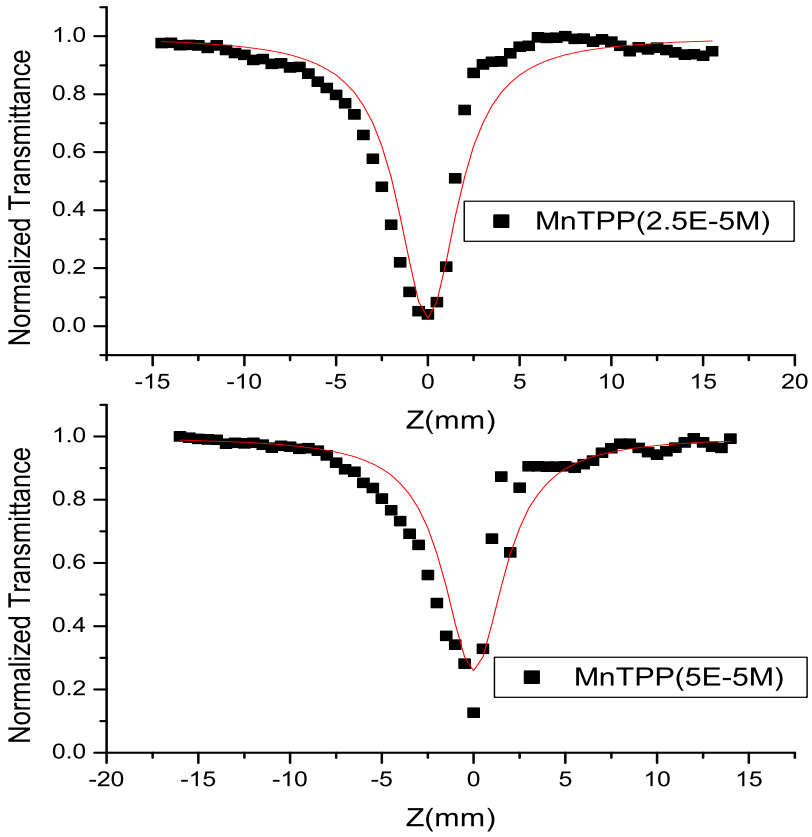

Figure 5.7: Z-scan of MnTPP in Nafion along with the fitted function (solid line) on the data for concentrations of (a)5*10^{-5}M and (b)2.5*10^{-5}M.

Table 5.5: Linear and nonlinear absorption coefficients of MnTPP with their theoretical fitting errors.

Data	$\beta(\frac{cm}{MW})$	Fitting error			$\alpha(mm^{-1})$
		$\Delta\beta$	% error	χ^2	
MnTPP(5E-5M)	0.27782	0.00957	3.4	0.90155	9.84
MnTPP(2.5E-5M)	0.25288	0.01138	4.5	0.83341	

Conclusion

The Porphyrins incorporated within Nafion membrane show strong nonlinear absorption and optical limiting behaviors for a high intensity radiation (laser) of wave length 532nm. These behaviors depend on the amount of Porphyrins embedded within Nafion membrane. The larger the concentration of Porphyrins, the stronger the nonlinear absorption and optical limiting effects. It is also determined that the Porphyrins which are incorporated within Nafion membrane are well protected from degradation. The nonlinear absorption coefficients for the Porphyrins which are embedded within Nafion membrane is determined by fitting their Z-scan results with the theoretical fitting function obtained from Z-scan theory. The values are found to increase with the amount of Porphyrins incorporated. The linear absorption coefficients of the Porphyrins is determined from the Z-scan results by considering only low intensity regimes from the data. It is so because at low intensities there is no nonlinear effect, only linear absorption is taking place.

Bibliography

[1] R. Knize, Opt. Lett., 18, (1993) 1606 - 1608.

[2] P. Miles, Appl. Opt., 30, (1994) 6965 - 6979.

[3] P. Miles, Appl. Opt., 38, (1999) 566 -570.

[4] Pieter Neethling, Determining nonlinear optical properties using the Z-Scan technique., MSc. thesis, University of Stallenbosch, April 2005.

[5] P.W. Milonni and J.H. Eberly (1988), Lasers, Chapters 2, 8, 14, 17, 18. John Wiley and Sons, New York.

[6] Steinmann C.M. (1999), Development and characterization of a tunable laser source in the vacuum ultraviolet., MSc. Thesis, University of Stellenbosch, South Africa.

[7] Boyd, R.W. (1992), Nonlinear Optics, Chapter 2, Academic Press, London.

[8] M. U. Ajgaonkar, Nonlinear optical properties of nanostructures, Phd dissertation, New Jersey Institute of Technology, January 2001.

[9] Scheidt, Generation von solvatisierten electronen in alkoholen, Diplomarbeit, Technischen Universitat Munchen, Deutscheland, (2001).

[10] M. Sheik-Bahae, A.A. Said, Tai-Huei Wei, D. J. Hagan, E.W. Van Stryland, Sensitive measurement of optical nonlinearities using a single beam, IEEE Journal of Quantum Electronics, 26 (4), 760-769, 1990.

[11] D. Weaire, B.S. Wherrett, D.A.B. Miller and S.D. Smith, Effect of low power nonlinear refraction on laser beam propagation in InSb, Optics Letters, 4, pp 331-333, 1974.

[12] M. Sheik-Bahae , A.A. Said and E.W. Van Stryland (1989), High-sensitivity, single-beam n_2 measurements, Optics Letters, Vol. **14**, No. 17, pp. 955-957.

[13] Electro-optics Handbook, Edited by Ronald Waynant and Marwood Ediger, Chapter 13 Nonlinear Optics, by Gary Wood and Edward Sharp, McGraw Hill Publishers, 1993.

[14] K. Sendhil, C. Vijayan, M. P. Kothiyal, Opt. Mat., (19 Nov. 2004).

[15] F. Zhao, J. Zhang, M. Kaneko, J. Photochem. Photobiol. A: Chem., 53, (1998) 119.

[16] K. Kadish, K. Smith, R. Gullard, The Porphyrin Handbook, 6, Academic Press, New York, 2000, p. 30 (Chapter 41).

[17] S. Couris et al (1995), Journal of Physics B: Atomic, Molecular and Optical Physics, 28, pp. 4537-4554.

PHOTOVOLTAIC PROPERTIES OF A BULK HETROJUNCTION SOLAR CELL

By
Girma Hailu

A THESIS PRESENTED TO
THE SCHOOL OF GRADUATE STUDIES
ADDIS ABABA UNIVERSITY
IN PARTIAL FULFILLMENT OF THE REQUIREMENTS
FOR THE DEGREE OF

MASTER OF SCIENCE in PHYSICS

ADDIS ABABA, ETHIOPIA
APRIL 2007

ADDIS ABABA UNIVERSITY

DEAPRMENT OF PHYSICS

The undersigned hereby certify that they have read and recommend to the Faculty of Science for acceptance a senior project entitled "**Photovoltaic Properties of a Bulk Hetrojunction Solar Cell**" by **Girma Hailu Master of Science**.

Dated: April 2007

Supervisor: _____
Dr.Genene Tessema

Readers: _____

_____

This Work is Dedicated to
My Dear Mother: Askale Bereka

Table of Contents

List of Figures

Abstract

Bulk-heterojunction solar cells are increasingly becoming a promising alternative solar energy converting devices. They are attractive because of their low production cost. They are novel materials for thin film, flexible and large-scale production. In this research work we studied the photovoltaic properties of a solar cell made by mixing the conjugated polymers APFOGreen-6 and D-75 and blending them with PCBM. The parameters of the solar cell are determined from the J-V characteristics under white light illumination and the UV-Visible absorption spectrum. From the absorption spectrum of the cell it is observed that the active layer absorbs very well in the UV-Visible region of the spectrum. The open circuit voltage (V_{oc}), short circuit current density (J_{sc}), fill factor (FF) and power conversion efficiency (η) of the cell obtained from the J-V characteristics under illumination are 608mV, 0.365mA/cm^2, 0.48648 and 0.102%, respectively.

Chapter 1

Introduction

1.1 Conjugated polymers

Although many people do not probably realize it but everyone is familiar with polymers. They are all around us in everyday life: in rubbers, plastics, resins, adhesives, medicines, etc. Their common feature is the presence of long covalently bonded chains of small units, known as monomers. So, the behavior of a polymer highly depends on the monomeric unit, the chemical bond which hold the monomers together and the spatial orientation of the monomers. Polymers have very large molecular weights. Even if, it is the subject of continued debate, the minimum molecular weight for a molecule to be called as a polymer is 25,000g/mol or more. This is the minimum molecular weight required for good physical and mechanical properties for many important polymers [1]. Polymers can be classified depending on their polymeric unit. A polymer consisting of only one type of repeating unit is known as a homopolymer. On the other hand, a polymer consisting of two or more repeating units is called a copolymer or heteropolymer [2].

A very important class of polymers with alternating single and double Carbon-Carbon bonds (conjugation) in their main chains are called conjugated polymers, see figure-1.1. Conjugated polymers are naturally prevalent in plants and animals. The fascinating process of photosynthesis in green plants and the retina molecule of the eye are examples of how nature makes use of conjugated molecules.

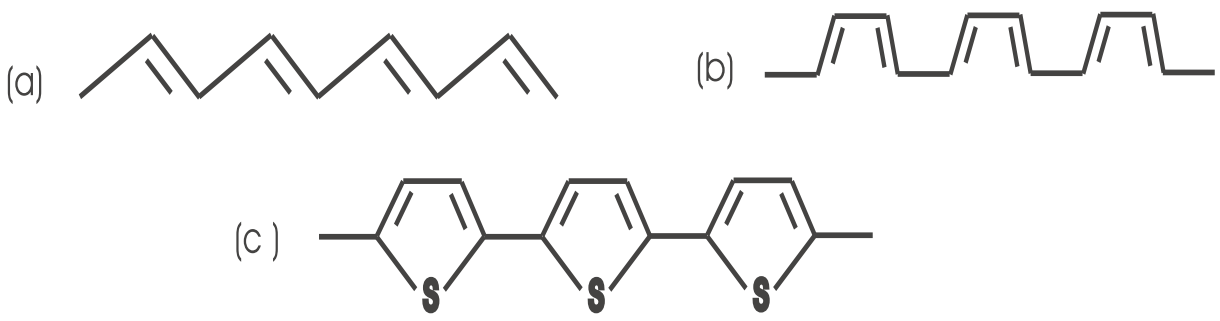

Figure 1.1: Conjugated Polymer Structure : (a) Trans- and (b)Cis-polyacetylene and (c) Polythiophene

Before the late 1970's organic polymers were classified as insulators. However; with the discovery of conducting polymers by 1970's, there was a genuine excitement about the possibility of producing materials that can combine the important electronic and optical properties of semiconductors and metals together with the attractive mechanical properties and easy processability of polymers[3]. Moreover, their conductivity can be tuned over 10 orders of magnitude through doping see figure 1.2. These properties of conducting polymers makes them to be promising materials in a number of important applications such as: chemical sensors[4], field effect transistors[5], micro-muscles[6], multi-color light-emitting diodes(LED$_s$)[7] and Solarcells[8].

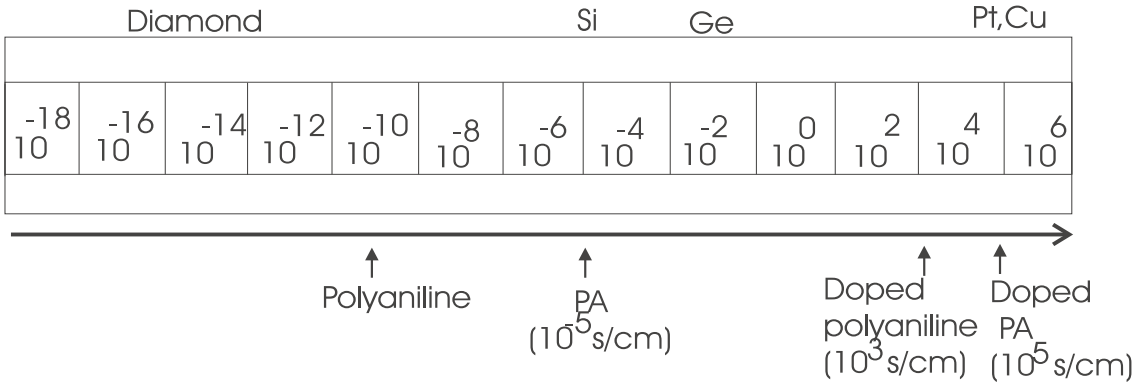

Figure 1.2: Range of conductivities of polymers compared with conductivities of other materials at room temperature.

1.2 Solar Cells

As the global energy demand continues to increase every year, the limiting supply of today's main energy sources (i.e. oil, coal, uranium) and their detrimental long-term effects on the natural balance of our planet, underscores the urgency of developing renewable energy sources which neither run out nor have any significant harmful effects on the environment. Harvesting energy directly from the sun using photovoltaic (PV) technology is being widely recognized as an essential component of future global energy production.

1.2.1 Inorganic Solar Cells

The photovoltaic cells have become extensively studied since the 1950s when the first crystalline silicon (Si) solar cell, which had efficiency of 6 percent was developed at Bell Laboratories [9]. Since then the efficiency continues to rise and has reached 24 percent for crystalline Si solar cells [10, 11]. At present, crystalline Si solar cells covers more than 85 percent of the photocell market.

Although the production of photovoltaic modules increases every year, it constitutes only a small portion of the total world energy production. This is due to large production cost for Si-based technology and limited availability of row materials such as solar-graded Si. Therefore, to ensure a sustainable energy technology for photovoltaic, the development of new materials and device structures are required.

1.2.2 Organic Solar Cells

Organic materials bear the potential to develop a long-term technology that is economically viable for large-scale power generation based on environmentally safe materials with unlimited availability.

The first generation of organic photovoltaic solar cells was based on single organic layers sandwiched between two metal electrodes of different work functions[12]. The power conversion efficiencies reported were generally poor (in the range of 10^{-3} to 10^{-1}). In 1986, Tang introduced the concept of bilayer hetrojunction solar cells and

obtained power conversion efficiency of about 1 percent [13]. With the introduction of bulk hetrojunction concept using a P-conjugated polymer and Fullerene (C_{60}) by Sariciftci et al. in 1992 [14], Yu et al. fabricated the first fully organic bulk hetrojunction photocell in 1995 using PCBM as an electron acceptor [15]. In 2001 Shaheen et al. obtained a power conversion efficiency of 2.5 percent from a bulk hetrojunction solar cell formed from the conjugated polymers MDMO-PPV and PCBM. Recently, power conversion efficiencies of $>$ 3.5 percent have been achieved for polymer : fullerene bulk hetrojunction solar cells based on Polythiophene derivatives such as P3HT [16].

In this report an organic bulk heterojunction solar cell is prepared by mixing the conjugated polymers D-75 and APFOGreen-6 and blending the mixture of polymers with the fullerene derivative PCBM. The reason behind mixing the polymers is to broaden the absorption spectrum which results to a more efficient solar cell. Since PCBM is highly soluble in chloroform and its electron affinity is high, it is very essential to dissociate the excitons formed following the absorption of light radiation. The efficiency and other parameters of the solar cell are determined from UV-Visible absorption and I-V characteristic measurements.

Chapter 2

Photoelectrical properties of Organic Photo Cells

2.1 Illuminated Current-Voltage Characteristics

For metal/semiconductor Schottky diodes, the dark current is mainly due to the majority carriers. But when the diode is illuminated with photons having enough energy for the creation of an electron-hole pair (exciton) in the depletion region, the electric field at the junction is able to separate the photogenerated charges by preventing recombination. So, the resulting photocurrent is mainly due to the minority carriers.

Suppose we have a metal/n-type polymer Schottky diode, there is an accumulation of holes at the semiconductor side of the interface in the dark. When light is illuminated, the concentration of holes in the semiconductor decreases due to recombination with photogenerated electrons. This results to the formation of new effective Fermi-level ($E_{f,eff}$) when equilibrium is attained. The total current under illumination is the sum of the photogenerated current and the thermally emitted current. Generally, the I-V characteristic of a photovoltaic device can be described by [19] :

$$I = I_o \left\{ \exp\left(\frac{e}{nkT}(V - IR_s)\right) - 1 \right\} + \frac{V - IR_s}{R_{sH}} - I_{pH} \tag{2.1}$$

Where I_o is the dark saturation current, e the elementary charge, n the diode ideality factor, V the applied voltage, R_s the series resistance, R_{sH} the shunt resistance, and

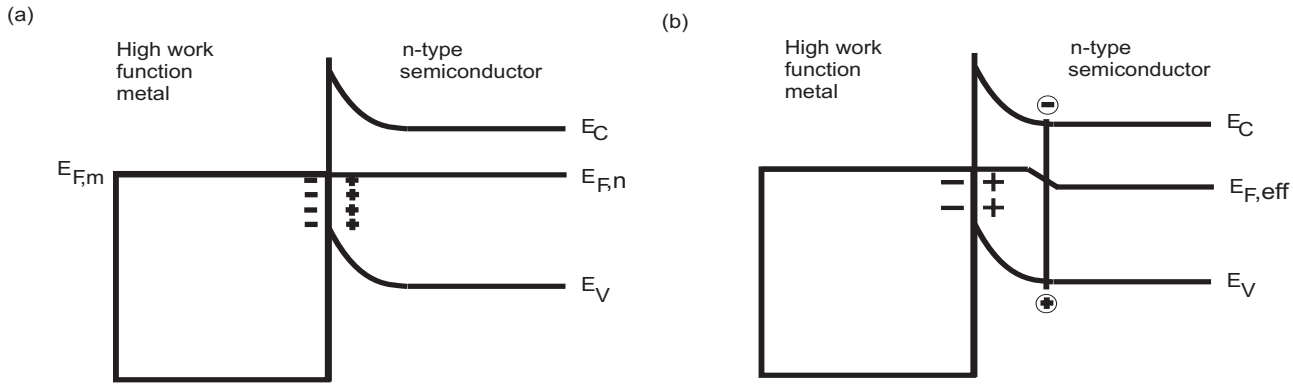

Figure 2.1: Energy band diagram of metal-semiconductor(n) (a) in the dark and(b) under illumination.

I_{pH} is the photocurrent. The corresponding equivalent circuit diagram is depicted in figure 2.2(b). For highly efficient solar cells R_{sH} is very large to prevent leakage current and the series resistance is very low to get a sharp rise in the forward current. So for this case equation 2.1 can be simplified to

$$I \;=\; I_o \left\{ \exp\left(\frac{eV}{nkT}\right) \;-\; 1 \right\} -\; I_{pH} \tag{2.2}$$

2.2 Spectral Response

The response of an organic photocell for the action of different spectrum of light radiation is different. That is, light of different wave lengths is absorbed to different depth in the photoactive layer. The intensity of light at a distance x in a uniform medium of absorption coefficient α, is given by

$$I(x) \;=\; I_o \, \exp\left[-\alpha(\omega)\, x\right] \tag{2.3}$$

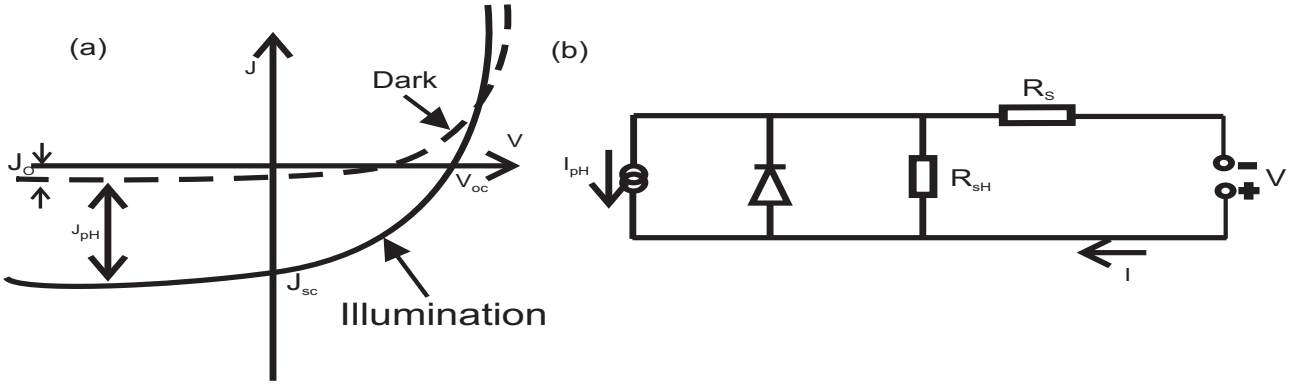

Figure 2.2: Figure (a) current-voltage characteristics of a photocell in the dark and under illumination (b) Equivalent circuit diagram for a solar cell, described by equation 2.1

Where I_o is the intensity inside the medium at $x = 0$ and ω is the frequency of light [40]. It should be remembered that

$$\omega(\lambda) = \frac{2\pi c}{\lambda} \tag{2.4}$$

Where λ and c are the wave length and the speed of light in vacuum, respectively. However, not all of the absorbed photons results to photocurrent, which is the desired product for photo cells. This limits the efficiency of the cells. The ability of a photo cell to generate photo current at a given wave length of the incident light is measured by the incident monochromatic photon to current conversion efficiency (IPCE). IPCE is defined as the number of photogenerated electrons per number of incident photons. It can be obtained from the photocurrent by means of the following equation [21].

$$IPCE\,0/0 = 1240\,\frac{J_{sc}}{\lambda I_i} \tag{2.5}$$

Where J_{sc} is the short-circuit photocurrent density (μA/cm^2), λ is the excitation wave length (nm), and I_{in} is the intensity of incident light (w/m^2). Plots of IPCE versus wave length illustrate the spectral operation range of a specific solar cell.

For organic photo cells which have rectifying contact at one of the electrodes (front

side) and ohmic contact at the other electrode (back side) like in single layer photo cells, the action spectra depends on which side, the cell is illuminated. For front side illumination, the strongly absorbed light creates Excitons in the barrier region. The internal electric field in the barrier region dissociates the Excitons and give rise to photocurrent. Under this conditions,the absorption spectrum is usually well matched with the action spectrum. For back side illumination, the strongly absorbed light produce Excitons in the field free bulk region. Whereas, the weakly absorbed photons penetrate in to the depletion region and make a major contribution to the photocurrent. If the polymer film is not thin enough, the Excitons from the strongly absorbed photons does not result to photocurrent due to recombinations or traps. The spectral response then does not correspond to the optical absorption spectra. The comparison of the action spectra with the absorption spectrum can be used to detect the active junction of photocells.

The efficiency of an organic photocell varies with the thickness of the polymer. For thin films (usually between 10-15nm), the efficiency increases as the thickness increases which is caused by the increase in the amount of sun light absorbed. However, the efficiency starts to decrease as the thickness becomes relatively large (around 50nm) because of the high density of traps in the film that reduce the number of carriers on their way to the active junction. Since these two competing processes are opposed to each other, there should be an optimum thickness for the maximum sun light conversion efficiency.

2.3 Fill Factor and Power Conversion Efficiency

Fill factor (FF) and power conversion efficiency (η) are among the parameters that characterize a solar cell. Fill factor tells about the squareness of the fourth quadrant of the I-V curve under illumination. Mathematically, it is defined as :

$$FF = \frac{I_{max}V_{max}}{I_{sc}V_{oc}} = \frac{P_{max}}{I_{sc}V_{oc}} \tag{2.6}$$

Where I_{max} and V_{max} are corresponding current and voltage values at the point where their product (power) is the maximum (P_{max})of all corresponding products of current

and voltages in the fourth quadrant of the I-V curve under illumination. I_{sc} and V_{oc} are short circuit current and open circuit voltages, respectively, see figure 4.3.

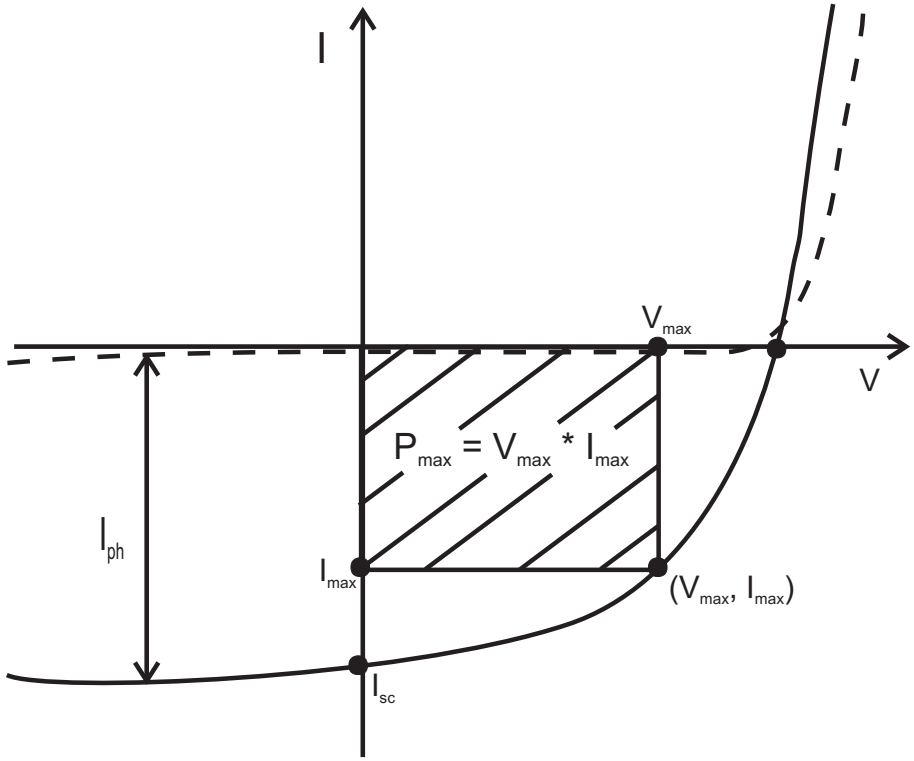

Figure 2.3: Typical I-V characteristics of an organic photo cell in the dark (dashed line) and illumination (solid line) conditions. The maximum out put power is given by the rectangle I_{max} * V_{max}.

The values of V_{max} and I_{max} can be computed from the following equation

$$\frac{\partial P}{\partial V}\Big|_{V=V_{max}} = 0 \tag{2.7}$$

For an ideal solar cell FF=1. For inorganic solar cells, the fill factor is typically between 0.7 and 0.8 [20]. For undoped organic semiconductor solar cells, it assumes values less than 0.7 [22].

The power conversion efficiency (η) of a solar cell is the ratio between the maximum

output power (P_{max}) and the power of incident light (P_{in}).

$$\eta \;=\; \frac{P_{max}}{P_{in}} \;=\; \frac{I_{sc}V_{oc}FF}{P_{in}} \tag{2.8}$$

In general, the conversion efficiency of a solar cell in percentage is given by [11, 20]

$$\eta\% \;=\; \left[\frac{I_mV_m}{P_{in}}\right] \times 100\,\% \tag{2.9}$$

or

$$\eta\% \;=\; FF\left[\frac{I_{sc}V_{oc}}{P_{in}}\right] \times 100\% \tag{2.10}$$

For organic solar cells based on polymer : Fullurene bulk heterojunctions, the magnitude of I_{sc}, V_{oc} and FF depends on parameters such as : light intensity [23], temperature [24], composition of the components [25], thickness of the active layer [26], the choice of the electrodes used [27], as well as the solid state morphology of the film [28].

Chapter 3

Experiment

3.1 Sample Preparation

The details of the sample preparation is stated as follows: a commercially obtained Indium Tin Oxide (ITO) coated glass is cut in to rectangular pieces of sizes 16mm by 20mm. The ITO is half etched using a warm solution of HNO_3:HCl:H_2O (1:1:4) by volume ratio, from substrate samples. These samples are first cleaned by detergents followed by Acetone. After that the glasses were rinsed in to Ethanol for about 10 minutes. As a final step of the cleaning process, the glasses were washed with distilled water and allowed to dry. A PEDOT-PSS solution is spin coated on the half etched ITO coated glasses while the spin coater is spinning at a rate of 3000rpm. In the other side a 5mg/ml solution using the conjugated polymers D-75 and APFOGreen-6 and PCBM with a weight ratio of (1:1:3) as solute and chloroform as solvent was prepared. The Polymer solution was then spin coated on the top of PEDOT-PSS, in this case the spinner's speed was 1000rpm. Finally, Aluminium (Al) was deposited on the top of the active layer (Polymer thin film) using Edward's auto vacuum depositor. Now, the sample is ready as schematically shown in figure-3.1 for further characterization.

It should be noted that through out the sample preparation and characterization steps, care must be taken not to expose the sample for light, moisture and contaminants.

Devices used for characterizing the solar cell are Perkin Elmer λ-19 Photospecrometer and HP-4140B Pico-Ameter/DC Voltage Source which is interfaced with a computer

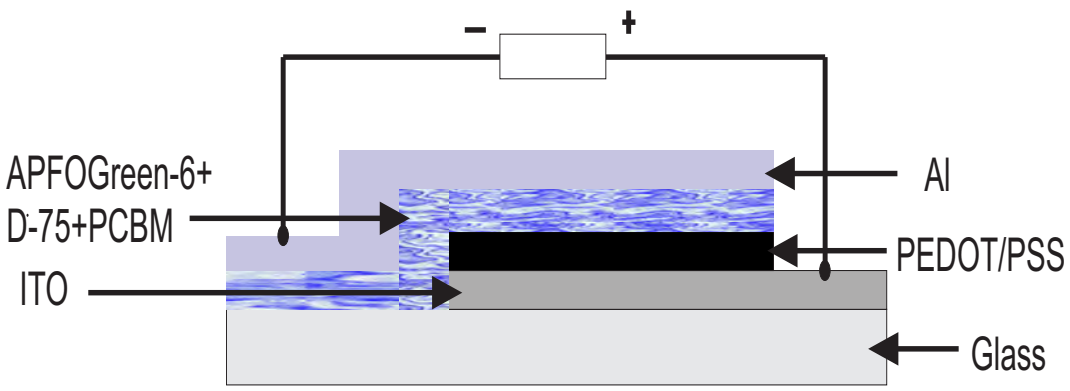

Figure 3.1: A schematic diagram of the photovoltaic devise used in this study.

through LabView programming software.

3.2 UV-Visible Absorption Measurement

It is known that the absorption spectrum of a material provide a lot of information including its energy levels. From the absorption spectrum of a semiconductor its energy band gap can be determined. When talking about solar cell the absorption spectrum of the active material which is absorbing the solar radiation is very crucial. It is so because most of the intensity of the solar radiation reaching on the earth's surface is found in the UV-Visible range of the light spectrum (see figure-3.2) [29]. This fact initiates the need for active materials which absorb quite well in this spectral range of interest. Due to the presence of π-electrons in the conjugation length of the conjugated polymers, a significant portion of the UV-Visible range of the spectrum is expected to be absorbed. Besides, the absorbance of a material depends on the amount (concentration) of absorbing molecules. In case of organic solar cells, the thicker the active layer the higher its absorbance.

3.3 I-V characteristic Measurement

Many of the parameters of a solar cell are extracted from its I-V characteristics. From the I-V characteristics under dark it is possible to tell about the type of junction

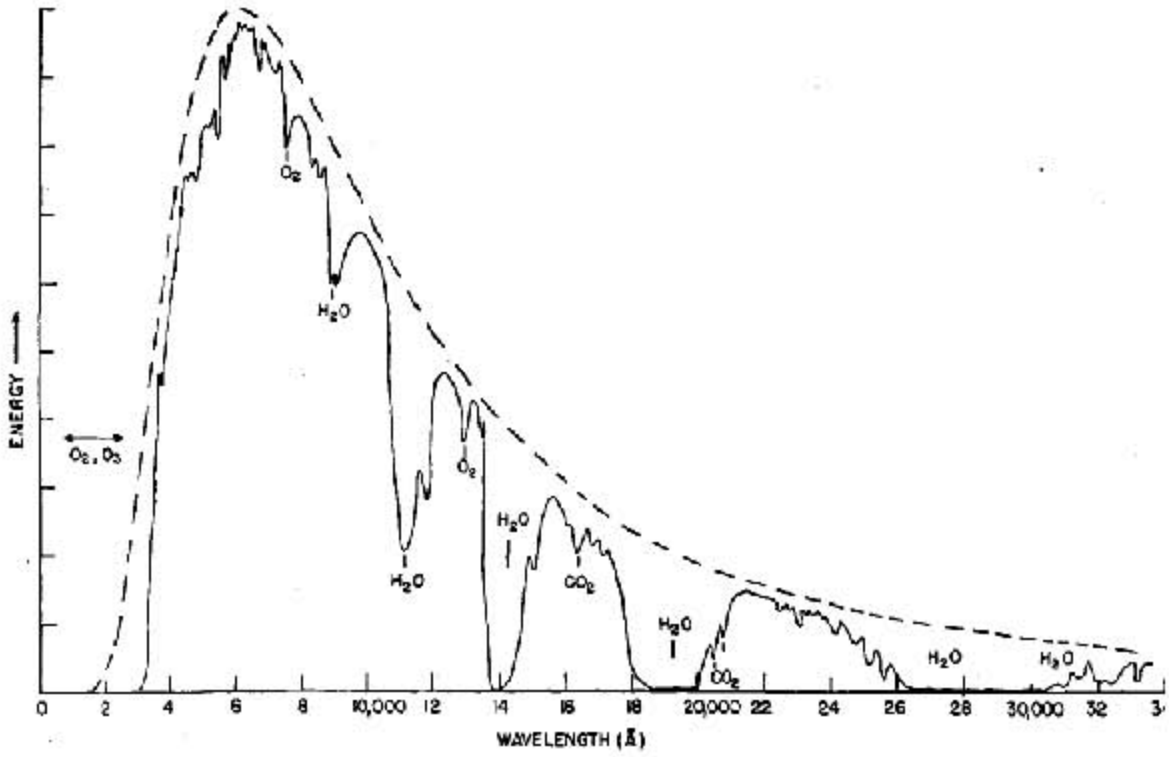

Figure 3.2: Spectral distribution of sun light arriving at Earth's surface [29].

formed between the active layer and the electrodes. Since the charge transport mechanism highly depends on the type of junction at the electrodes, this I-V characteristic will give information about the mechanism which govern the charge carrier transport at the junction. Important parameters of a solar cell like open circuit voltage (V_{oc}), short circuit current (I_{sc}), Fill Factor (FF) and power conversion efficiency (η) are determined from its I-V characteristics under illumination.

As shown in section 2.3 the I-V characteristics under illumination showed a shift down wards as it is compared with the I-V characteristics under dark due to photogenerated currents. The I-V curve under illumination form an area in the fourth

quadrant which provides all the parameters that are stated above.

Chapter 4

Results and Discussion

4.1 UV-Visible Absorption Spectrum Result

The sample used for the UV-Visible absorption measurement is some how different in its preparation than the one whose preparation is explained in section 3.1. In this case pure transparent glasses of sizes 20mm by 20mm are used as substrates for the active layer which is spin coated at a speed of 1000rpm. The absorption spectrum of the film in the UV-Visible range is shown in figure-4.1. The figure shows a significant absorption in this region of the spectrum to be used as light absorbing agent for the solar cell.

As it can easily be seen from figure 4.1 the absorption decreases in the region of higher wave lengths (between 425nm to 800nm) and increases in the region of lower wave lengths (between 250nm to 420nm) due to the addition of PCBM. This behavior continues to magnify as the proportion of PCBM with the polymers is increased which in effect decreases the efficiency of the cell. On the other hand, more PCBM is needed to dissociate the exciton formed following the absorption of photons by the polymers. So, it is very important to choose an optimum proportion of PCBM which compromises these seemingly contrasting behaviors and results to a more efficient solar cell.

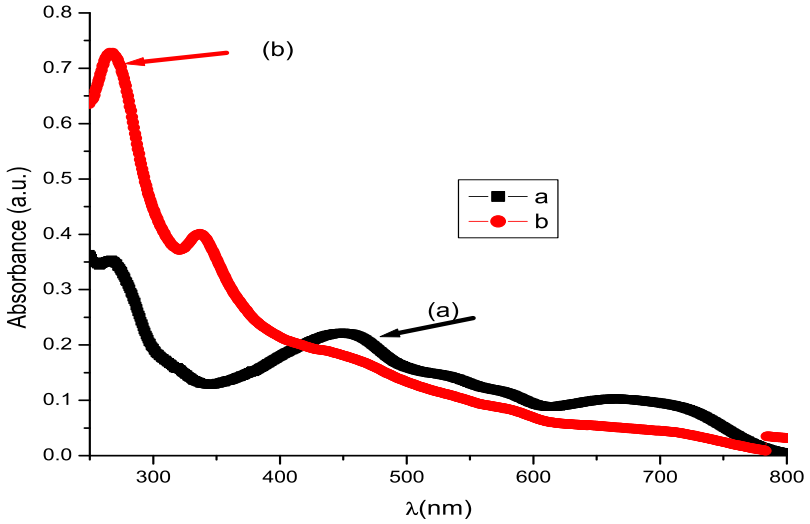

Figure 4.1: Absorption Spectrum of the conjugated polymers D-75+WM-419 (a) with out and (b) with PCBM.

4.2 I-V Characteristic Result

Figure-4.2 shows the I-V characteristics under white light illumination for the solar cell. From the figure the open circuit voltage (V_{oc}) is obtained by taking the value of the abscissa where the current is zero (the point where the graph crosses the horizontal axis) which is found to be 0.608V. By taking the value of the ordinate at the point where the graph crosses the vertical axis, the short circuit current density (J_{sc}) is determined to be 0.365mA/cm^2. The maximum possible power (P_{max}) that can be generated by the solar cell is obtained by taking the maximum product of all corresponding current and voltage values which are found in the fourth quadrant of the graph, see section 2.3. The ratio of P_{max} to the product of V_{oc} and I_{sc} results to the Fill Factor (FF) of the cell which is found to be 0.486. By measuring the intensity of input white light that is normally incident on the ITO side using the Lux-Meter; taking the above values of V_{oc}, J_{sc} and FF and using equation-2.10, the power conversion efficiency of the cell is determined to be 0.102%.

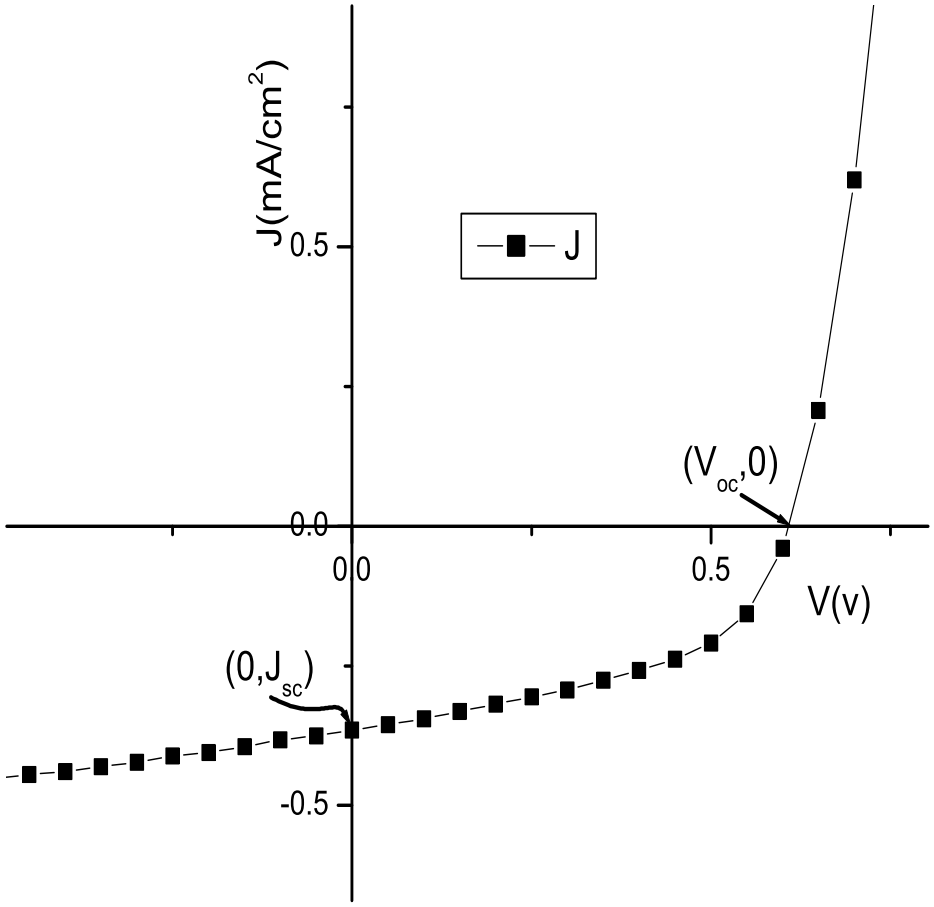

Figure 4.2: I-V Characteristics of a solar cell under white light illumination

Conclusion

A bulk heterojunction organic solar cell is prepared by using the conjugated polymers D-75 and APFOGreen-6 as light absorbing materials. A Fullerene derivative PCBM is blended with the polymers since it is very essential to dissociate the excitons formed following the absorption of light by the polymers. The open circuit voltage of the cell is determined to be 0.608V. The corresponding short circuit currents and fill factors are 0.365mA/cm^2 and 0.486, respectively. The power conversion efficiency of the cell is determined to be 0.102%.

Bibliography

[1] L. H. Sperling, John Wiley and sons Inc., New York, 1986.

[2] Peter Nilsson, "Conjugated Polyelectrolytes: Conformation sensitive optical probes for the recording of biological processes", PhD. Dessertations, Linköping University, SE-581 83, Linköping, Sweeden, 2005.

[3] Azar Assadi Moghaddam, "Polymer Based Electronic Devices", PhD. Dessertations, Linköping University, SE-581 83, Linköping, Sweeden, 1993.

[4] A. Assadi, A. Spetz, M. Willander, C. Svensson, I. Lundström and O. Inganäs, "Sensors and Actuators", B 20, 1994, 71.

[5] A. Assadi, M. Willander, C. Svenson and J. Hellberg, Synth. Met. 53, 1993, 187.

[6] E. Smela, O. Inganäs and I. Lundström, Science, 268 (1995) 1735.

[7] Berggren, O. Inganäs, G. Gustafsson, J. Rasmusson, M.R. Anderson, T. Hjerberg and O. Wennerström, Nature 372 (1994) 444.

[8] A. Gadisa, B. Workalemahu, synthetic metals 129, 179-185.

[9] D. M. Chapin, C. S. Fuller, G. L. Pearson, Journal of Applied Physics 25 (1954), 676.

[10] M. A. Green, K. Emery, D. L. King, S. Igari,W.Warta, Solar cell efficiency tables (version 25), Progress in Photovoltaics 13 (2005), 49.

[11] W. Shockley, H. J. Queisser, Journal of Applied Physics 32 (1961), 510.

[12] G.A. Chamberlain, Organic solar cells: A review, Solar Cells 8, 47 (1983).

[13] C.W. Tang: Two-layer organic photovoltaic cell. Appl. Phys. Lett. 48, 183 (1986).

[14] N. S. Sariciftci, L. Smilowitz, A. J. Heeger, Science 258 (1992), 1474.

[15] G. Yu, J. Gao, J. C. Hummelen, F. Wudl, A. J. Heeger, Science 270 (1995), 1789.

[16] D. Chirvase, J. Parisi, J. C. Hummelen, V. Dyakonov, Nanotechnology 15 (2004), 1317.

[17] H. Hoppe etal., Organic Solar Cells: An overview, J. Mater. Res., Vol. 19, no. 7, July 2004.

[18] Peter W. Milloni and Joseph H. Eberty, Lasers, John Wiley and Sons, New York, 1988.

[19] N. Vlachopoulos, P. Liska, J. Augustynski and M. Grätzel, J. Ame. Chem. Soc., 110 (1988), 1216.

[20] Donald A. Neamen, Semiconductor Physics and Devices: Basic Principles, Richard D. IRWIN, inc., 1992.

[21] M. S. Roy, G. D. Sharma and S. G. Sangodkar, Synth. Met., 81 (1996) 15.

[22] Donald A. Seanor, Electrical Properties of Polymers, Academic Press, New York, 1982.

[23] P. Schilinsky, C. Waldouf, C. J. Brabec, Appl. Phys. Lett. 81 (3885), 2002.

[24] V. Dyakonov, Electrical Aspects of Operation of Polymer-Fullerene Solar Cells, Thin films 451-52 (2004), 493.

[25] J. K. J. Van Duren, X. N. Yang, J. Loos, C. W. T. Bulle-Lieuwma, A. B. Sieval, J. C. Hummelen, R. A. Janssen, Advanced Functional Materials, 14 (2004), 425.

[26] H. Hoope, N. Arnold, N. S. Sariciftci, D. Meissner, Solar energy materials and Solar Cells, 80, 105, (2003).

[27] C. J. Brabec, A. Cravino, D. Meissner, N. S. Sariciftci, M.T. Rispens, L. Sanchez, J. C. Hummelen, T. Fromhertz, Thin Solid films, 403, 368, (2002).

[28] S. E. Shaheen, C. J. Brabec, N. S. Sariciftci, F. Padinger, T. Fromhertz, J. C. Hummelen, Appl. Phys. Lett., 78, 841, (2001).

[29] John H. Shaw, Solar Radiation, The Ohio Journal of Science 53 (5): 258, September, 1953.

DECLARATION

I the under signed declare that the thesis is my original work, has not been presented for a degree in any other university and that all sources of material used for the thesis have been duly acknowledged.

Name: _____

Signature: _____

This Thesis has been submitted for examination with my approval as university advisor.

Name: _____

Signature: _____